

ORIGINAL RESEARCH

# Highly Selective PPAR $\alpha$ (Peroxisome Proliferator-Activated Receptor $\alpha$ ) Agonist Pemafibrate Inhibits Stent Inflammation and Restenosis Assessed by Multimodality Molecular-Microstructural Imaging

Hiroshi Iwata , MD, PhD\*; Eric A. Osborn , MD, PhD\*; Giovanni J. Ughi, PhD\*; Kentaro Murakami, PhD; Claudia Goettsch, PhD; Joshua D. Hutcheson , PhD; Adam Mauskapf, BS; Peter C. Mattson, MD; Peter Libby , MD; Sasha A. Singh, PhD; Joan Matamalas , PhD; Elena Aikawa , MD, PhD; Guillermo J. Tearney, MD, PhD<sup>†</sup>; Masanori Aikawa , MD, PhD<sup>†</sup>; Farouc A. Jaffer , MD, PhD<sup>†</sup>

**BACKGROUND:** New pharmacological approaches are needed to prevent stent restenosis. This study tested the hypothesis that pemafibrate, a novel clinical selective PPAR $\alpha$  (peroxisome proliferator-activated receptor  $\alpha$ ) agonist, suppresses coronary stent-induced arterial inflammation and neointimal hyperplasia.

**METHODS AND RESULTS:** Yorkshire pigs randomly received either oral pemafibrate (30 mg/day; n=6) or control vehicle (n=7) for 7 days, followed by coronary arterial implantation of 3.5 × 12 mm bare metal stents (2–4 per animal; 44 stents total). On day 7, intracoronary molecular-structural near-infrared fluorescence and optical coherence tomography imaging was performed to assess the arterial inflammatory response, demonstrating that pemafibrate reduced stent-induced inflammatory protease activity (near-infrared fluorescence target-to-background ratio: pemafibrate, median [25th–75th percentile]: 2.8 [2.5–3.3] versus control, 4.1 [3.3–4.3],  $P=0.02$ ). At day 28, animals underwent repeat near-infrared fluorescence–optical coherence tomography imaging and were euthanized, and coronary stent tissue molecular and histological analyses. Day 28 optical coherence tomography imaging showed that pemafibrate significantly reduced stent neointima volume (pemafibrate, 43.1 [33.7–54.1] mm<sup>3</sup> versus control, 54.2 [41.2–81.1] mm<sup>3</sup>;  $P=0.03$ ). In addition, pemafibrate suppressed day 28 stent-induced cellular inflammation and neointima expression of the inflammatory mediators TNF- $\alpha$  (tumor necrosis factor- $\alpha$ ) and MMP-9 (matrix metalloproteinase 9) and enhanced the smooth muscle differentiation markers calponin and smoothelin. In vitro assays indicated that the STAT3 (signal transducer and activator of transcription 3)–myocardin axes mediated the inhibitory effects of pemafibrate on smooth muscle cell proliferation.

**CONCLUSIONS:** Pemafibrate reduces preclinical coronary stent inflammation and neointimal hyperplasia following bare metal stent deployment. These results motivate further trials evaluating pemafibrate as a new strategy to prevent clinical stent restenosis.

**Key Words:** coronary artery disease ■ inflammation ■ molecular imaging ■ optical coherence tomography ■ pemafibrate ■ restenosis ■ SPPARM $\alpha$  (selective peroxisome proliferator-activated receptor alpha modulator alpha)

Correspondence to: Farouc A. Jaffer, MD, PhD, Division of Cardiology, Massachusetts General Hospital, Simches 3206, 185 Cambridge Street, Boston, MA 02114. E-mail: fjaffer@mgh.harvard.edu and Masanori Aikawa, MD, PhD, Center for Interdisciplinary Cardiovascular Sciences, Brigham and Women's Hospital, 3 Blackfan St, CLSB, Floor 17, Boston, MA 02115. E-mail: maikawa@bwh.harvard.edu

\*H. Iwata, E.A. Osborn, and G.J. Ughi are co-first authors.

<sup>†</sup>G.J. Tearney, M. Aikawa, and F.A. Jaffer share senior authorship.

Supplementary Material for this article is available at <https://www.ahajournals.org/doi/suppl/10.1161/JAHA.121.020834>

For Sources of Funding and Disclosures, see page 10.

© 2021 The Authors. Published on behalf of the American Heart Association, Inc., by Wiley. This is an open access article under the terms of the Creative Commons Attribution-NonCommercial-NoDerivs License, which permits use and distribution in any medium, provided the original work is properly cited, the use is non-commercial and no modifications or adaptations are made.

JAHA is available at: [www.ahajournals.org/journal/jaha](http://www.ahajournals.org/journal/jaha)

## CLINICAL PERSPECTIVE

### What Is New?

- This is the first study to demonstrate that pemafibrate, a novel PPAR $\alpha$  (peroxisome proliferator-activated receptor  $\alpha$ ) agonist and selective PPAR $\alpha$  modulators can reduce coronary stent-induced vascular inflammation and neointima formation in pigs as measured by clinically translatable intravascular near-infrared fluorescence–optical coherence tomography molecular structural imaging.

### What Are the Clinical Implications?

- Restenosis remains a significant source of morbidity following coronary and peripheral intervention, and at present, there are limited oral pharmacotherapies to prevent restenosis.
- Study findings indicate that pemafibrate may merit evaluation as a new pharmacologic strategy to limit clinical endovascular stent restenosis.
- Intravascular near-infrared fluorescence–optical coherence tomography imaging may be a new translatable approach to evaluate the anti-inflammatory actions of new drugs in vivo in coronary arteries.

## Nonstandard Abbreviations and Acronyms

<b>BMS</b>	bare metal stent
<b>DES</b>	drug-eluting stent
<b>NIRF</b>	near-infrared fluorescence
<b>PPAR<math>\alpha</math></b>	peroxisome proliferator-activated receptor $\alpha$
<b>SMC</b>	smooth muscle cell
<b>TBR</b>	target-to-background ratio

**E**ndovascular stent implantation during percutaneous coronary intervention or peripheral artery disease (PAD) intervention provides a highly effective therapy for obstructive atherosclerosis. However, stent implantation induces vascular injury and inflammation that can incite excessive neointimal hyperplasia and clinical stent restenosis, a morbid and costly condition often leading to rehospitalization and repeat intervention and potentially increased mortality.<sup>1,2</sup> Furthermore, despite contemporary stent technology and optimized implantation techniques, metallic stents carry an indefinite risk of late failure attributed to both fibrotic neointima formation or neoatherosclerosis, characterized by neointima containing foamy macrophages, cholesterol clefts, and rupture-prone fibrous caps.<sup>3,4</sup> Therefore,

new strategies to reduce stent restenosis remain urgently needed.

At present, no oral pharmacotherapies effectively prevent clinical restenosis.<sup>5</sup> As inflammation and cellular proliferation play a crucial role in neointima formation,<sup>6,7</sup> therapeutics inducing both anti-inflammatory and antiproliferative effects might potently inhibit restenosis. This study investigated a new anti-inflammatory and antiproliferative strategy using the novel clinical oral agent pemafibrate, a highly selective PPAR $\alpha$  (peroxisome proliferator-activated receptor  $\alpha$ ) agonist.<sup>8</sup> Pemafibrate represents a new class of drugs: selective PPAR $\alpha$  modulators that favorably alter lipoprotein levels.<sup>9</sup> In addition to its lipid modulatory capacity, PPAR $\alpha$  activation may also exert anti-inflammatory and antiatherogenic effects,<sup>10–12</sup> but its effects on restenosis are undetermined.

This preclinical in vivo molecular-structural inflammation imaging and biological investigation tested the hypothesis that selective PPAR $\alpha$  activation with pemafibrate can suppress in vivo stent-induced inflammation and neointima formation in pig coronary arteries as assessed by intravascular near-infrared fluorescence (NIRF)–optical coherence tomography (OCT) hybrid imaging.<sup>13–15</sup> To further understand the potential antirestenosis effects of pemafibrate, we investigated anti-inflammatory and antiproliferative cellular and molecular mechanisms in cellular and organ cultures.

## METHODS

The authors declare that all supporting data are available within the article (and its online supplementary files).

### Study Protocol

This study was approved and performed in compliance with the Massachusetts General Hospital Institutional Animal Care and Use Committee (protocol number 2012N000066). Healthy male Yorkshire pigs (2.6 $\pm$ 0.3 months old, body weight 25–30 kg, N=13) were fed normal chow and then randomized to receive oral pemafibrate or PBS 7 days before bare metal stent (BMS) implantation (3.5  $\times$  12 mm, Multi-Link Vision, Abbott Vascular) into a coronary artery at a 1.3:1 stent: artery overexpansion ratio guided by intravascular ultrasound (IVUS), which was followed by dual antiplatelet therapy. Based on a previous pilot pharmacokinetics study of pemafibrate in normal pigs, a dose of approximately 1 mg/kg/day (30 mg/day) per pig was chosen for this study. BMSs were used to generate more abundant restenosis compared with drug-eluting stents (DESs) that harbor embedded antiproliferative coatings. Pigs next underwent serial intravascular NIRF-OCT imaging at days 7 and 28 after stent implantation (Figure S1). Following day 28 imaging, pigs were euthanized, and excision of the coronary arteries

on ice occurred within 15 minutes. Arteries were then processed for histopathology, quantitative polymerase chain reaction, immunoblotting, and proteomic assays.

### Intracoronary Molecular-Structural Imaging

Intravascular NIRF-OCT and IVUS imaging were performed in all animals on days 7 and 28 after stent implantation (Figure 1). In addition, day 7 NIRF-OCT imaging was performed in a subgroup of animals (3 of 7 control animals and 3 of 6 pemafibrate animals). To visualize stent cathepsin proteinase inflammatory activity in vivo, intravenous ProSense VM110 (60 mg/pig,  $2.1 \pm 0.1$  mg/kg, PerkinElmer), a NIRF cathepsin protease activity reporter, was administered 24 hours before NIRF-OCT imaging.<sup>13,16,17</sup> ProSense VM110 (ex/em 750 nm/770 nm) is optically silent in its native state, but after lysine-lysine bond cleavage by cathepsin B, L, or S proteases, generates strong local NIR fluorescence.<sup>13,16,17</sup> Data S1 provides additional details of the NIRF-OCT imaging apparatus.

### Histologic Examination, Protein Isolation and Proteomics Analysis, Quantitative Real-Time Polymerase Chain Reaction, Ex Vivo Carotid Artery Ring Organoid Culture, and Primary Smooth Muscle Cell Culture

Detailed methods are described in Data S1.

### Statistical Analysis

Data are presented as median (25th–75th percentiles) or mean $\pm$ SD as appropriate. An “n” indicates the number of independent experiments or number of animals/samples. Tests with a *P* value < 0.05 were considered statistically significant. Pairwise group comparisons were performed using a non-parametric Mann–Whitney *U* test (SPSS 24, IBM Corp., Armonk, NY, and GraphPad Prism 5, Prism Software Inc, La Jolla, CA). Linear correlation between 2 parameters was performed to calculate the Spearman’s correlation coefficient (*r*). Factorial repeated-measures ANOVAs as mixed models using a random intercept for each pig and an interaction between terms (treatment and level) were performed for comparisons between the pemafibrate and control groups of OCT-derived percent stenosis in 36 levels/positions per stent (a total of 1584 OCT images analyzed across 44 stents; 24 control and 20 pemafibrate).

## RESULTS

### Pemafibrate Suppresses Stent-Induced Inflammatory Protease Activity in Pig Coronary Arteries as Assessed by NIRF-OCT Hybrid Imaging In Vivo

After stent implantation, intravascular images revealed similar stent overexpansion at day 0 and at day 7 between groups (stent diameter : distal reference

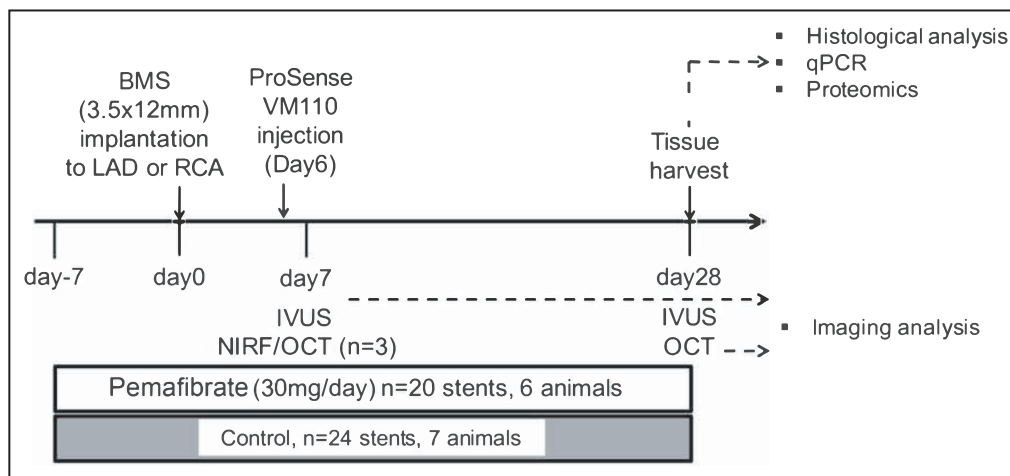


**Figure 1. Study scheme and analysis protocol. Pemafibrate administration (30 mg/animal/day) was initiated at day –7 and continued until animals were harvested at day 28 (total 35-day protocol).**

On day 0, BMSs (3.5 × 12 mm) were deployed into the pig RCA and LAD coronary arteries. Arterial injury was induced by stent balloon overinflation under IVUS guidance. Intravascular imaging using IVUS and NIRF-OCT was performed on day 7 at 24 hours after intravenous injection of ProSense VM110, a NIRF molecular imaging reporter of cathepsin protease activity. Tissues were harvested at day 28 for analysis. BMS indicates bare metal stent; IVUS, intravascular ultrasound; LAD, left anterior descending coronary artery; NIRF, near-infrared fluorescence; OCT, optical coherence tomography; qPCR, quantitative polymerase chain reaction; and RCA, right coronary artery.

diameter ratios of 1.34–1.39; Table S1) without medial dissection, intramural hematoma, or strut malapposition. The day 7 inflammatory protease activity monitored in vivo by the NIRF imaging agent ProSense VM110, an established cathepsin protease activity reporter in arterial disease,<sup>13,17</sup> was captured during NIRF-OCT imaging. The 3-dimensional coronary artery NIRF signals were displayed on a 2-dimensional NIRF map and quantified as the ratio of NIRF intensities in the lesion of interest to those in the nonstented regions (target-to-background ratio [TBR]). Pemafibrate administration reduced the NIRF cathepsin protease inflammation signal localized in the stented coronary artery at day 7 compared with stents implanted in control pigs (Figure 2A). The NIRF inflammation TBR in the pemafibrate treated group (TBR, 2.8 [2.5–3.3]; 9 stents and 3 animals) was significantly lower than the control group (TBR, 4.1 [3.3–4.3]; 9 stents and 3 animals;  $P=0.024$ ; Figure 2B).

### Pemafibrate Reduces Neointimal Hyperplasia in Stented Arteries

On day 28, in vivo intracoronary OCT images (44 stents and 13 animals) and Movat's pentachrome stain of histological sections (13 stents and 13 animals) enabled the quantification of the stent neointima area (Figure 3A). Manual measurements of the coronary lumen and the stent cross-sectional area by OCT yielded a 3-dimensional quantitative evaluation of the neointima volume per stent in the pemafibrate and control groups. Neointima volume at day 28 was lower in the arteries of pemafibrate-treated pigs than controls (control, 54.2 [41.2–81.1] mm<sup>3</sup> versus pemafibrate, 43.1 [33.7–54.1] mm<sup>3</sup>;  $P=0.032$ ; Figure 3B). Longitudinal analysis by comparison in 2 groups using factorial-measures ANOVAs with mixed models further showed a significantly lower percent luminal stenosis in stents in the pemafibrate group, particularly at the distal edge of the stent ( $P<0.001$ ). Analyses on a per-stent basis by OCT showed significantly lower neointima volume, percent area, and volume stenosis in the pemafibrate group (Figure 3B, 3C, 3F, and 3G), whereas there was nonsignificant lower neointimal area and volume in the pemafibrate group on a per-animal analysis of the OCT and histology data (Figure 3D, Figure S1a and 1b). Moreover, the NIRF protease activity TBR on day 7 correlated moderately with the day 28 neointima volume per stent ( $r=0.52$ ,  $P=0.031$ ), indicating that early stent-induced NIRF inflammation may be able to predict the degree of subsequent stent neointima hyperplasia (Figure 3E). Both the day 28 OCT-derived stent mean percent neointima area stenosis (Figure 3F) and percent neointima volume (Figure 3G) were significantly lower in stents of pemafibrate-treated animals.

### Effects of Pemafibrate on Body Weight, Triglyceride, and Hepatic Enzymes

At 2 to 6 hours after oral administration, the plasma pemafibrate concentration was measured at 38.2±32.8 ng/dL, whereas it was undetectable in the plasma of controls. Pemafibrate did not alter body weight during the 35-day study. Although pemafibrate was developed as a clinical triglyceride-lowering drug, the dose we chose did not significantly change triglyceride levels at day 28 (35 days after treatment initiation) in normolipidemic pigs (14.4±6.9 mg/dL in the controls, 12.6±7.5 mg/dL in the pemafibrate group, and 17.8±1.8 mg/dL in normal Yorkshire pigs<sup>18</sup>) who had low triglyceride concentrations at baseline. Pemafibrate did not induce hepatic enzyme elevation at day 28 (35 days of administration), including aspartate aminotransferase (25.6±15.0 U/L in the controls, 14.9±6.4 U/L in the pemafibrate group, and 48.9±10.5 U/L in normal Yorkshire pigs<sup>19</sup>) and alanine aminotransferase (39.7±7.0 IU/L in the controls, 43.3.1±11.7 IU/L in the pemafibrate group, and 50.5±4.9 IU/L in normal Yorkshire pigs<sup>19</sup>), indicating no apparent hepatic toxicity at the administered dose (Table S2).

### Pemafibrate Suppresses Cell Accumulation and Proliferation in Stented Arteries

The stented coronary arteries of pemafibrate-treated animals at day 28 demonstrated that for a given amount of neointima, there was higher  $\alpha$ -smooth muscle actin (SM $\alpha$ -actin) area and fewer Ki-67-positive nuclei, a marker of cell proliferation (Figure 4A). Double immunofluorescence staining of Ki-67 and SM $\alpha$ -actin indicated that pemafibrate suppressed the accumulation of proliferating Ki-67+ cells while increasing the presence of mature SM $\alpha$ -actin+ smooth muscle cells (SMCs). Colocalization analysis (Figure 4A) further showed that most Ki-67 cells were not SM $\alpha$ -actin positive, suggesting that Ki-67+ cells may be inflammatory cells or less-differentiated SMCs. Fewer cells were present in the pemafibrate group on a per-strut basis (N=504 control, N=432 pemafibrate [Figure 4B, left];  $P=0.016$ ) as well as on a per-animal basis (N=7 control, N=6 pemafibrate, 72 stent struts analyzed per animal [Figure 4B, right];  $P=0.008$ ). Moreover, histological analysis demonstrated that pemafibrate reduced the strut-associated inflammation, granulomatous inflammation, and vascular injury scores (all  $P<0.05$ ; Figure 4C through 4E). These findings illustrate that pemafibrate suppressed stent injury-induced cell accumulation and proliferation. At day 28, we observed a positive correlation between the day 28 stent-induced granulomatous inflammation and neointimal area (Figure S2b;  $r=0.24$ ,  $P=0.03$ ). No statistically significant

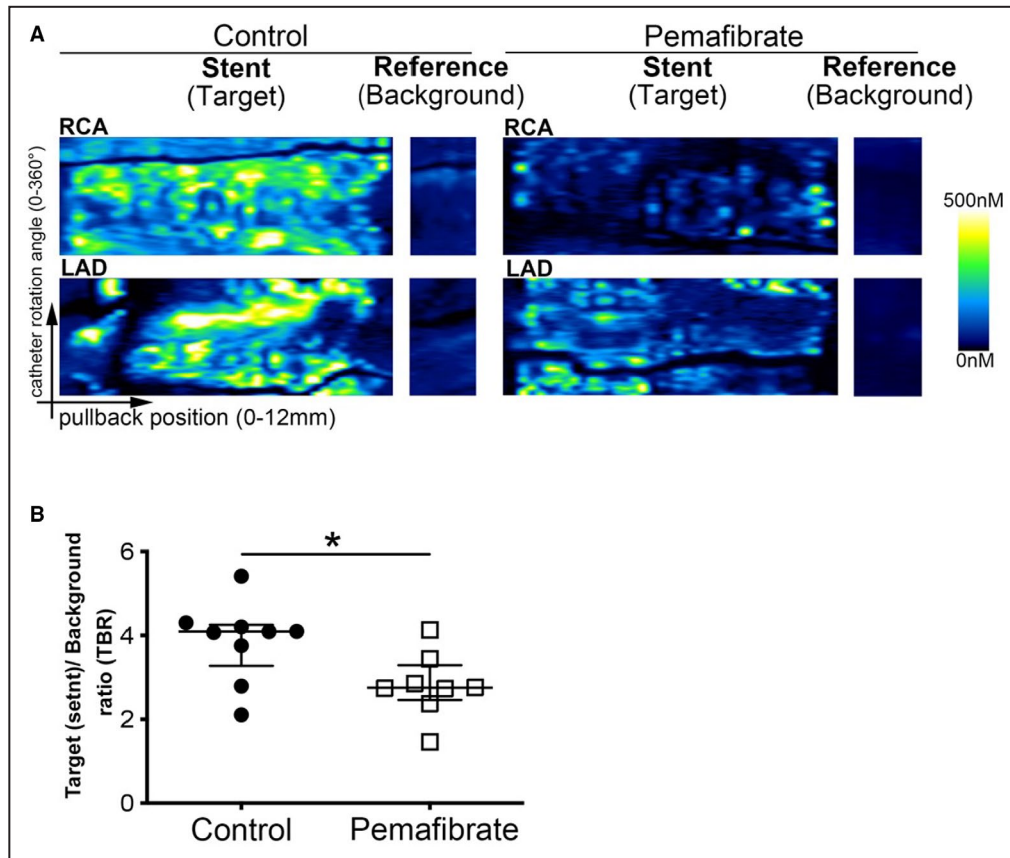


**Figure 2.** The effects of pemafibrate on in vivo arterial inflammatory cathepsin activity 7 days after stent implantation.

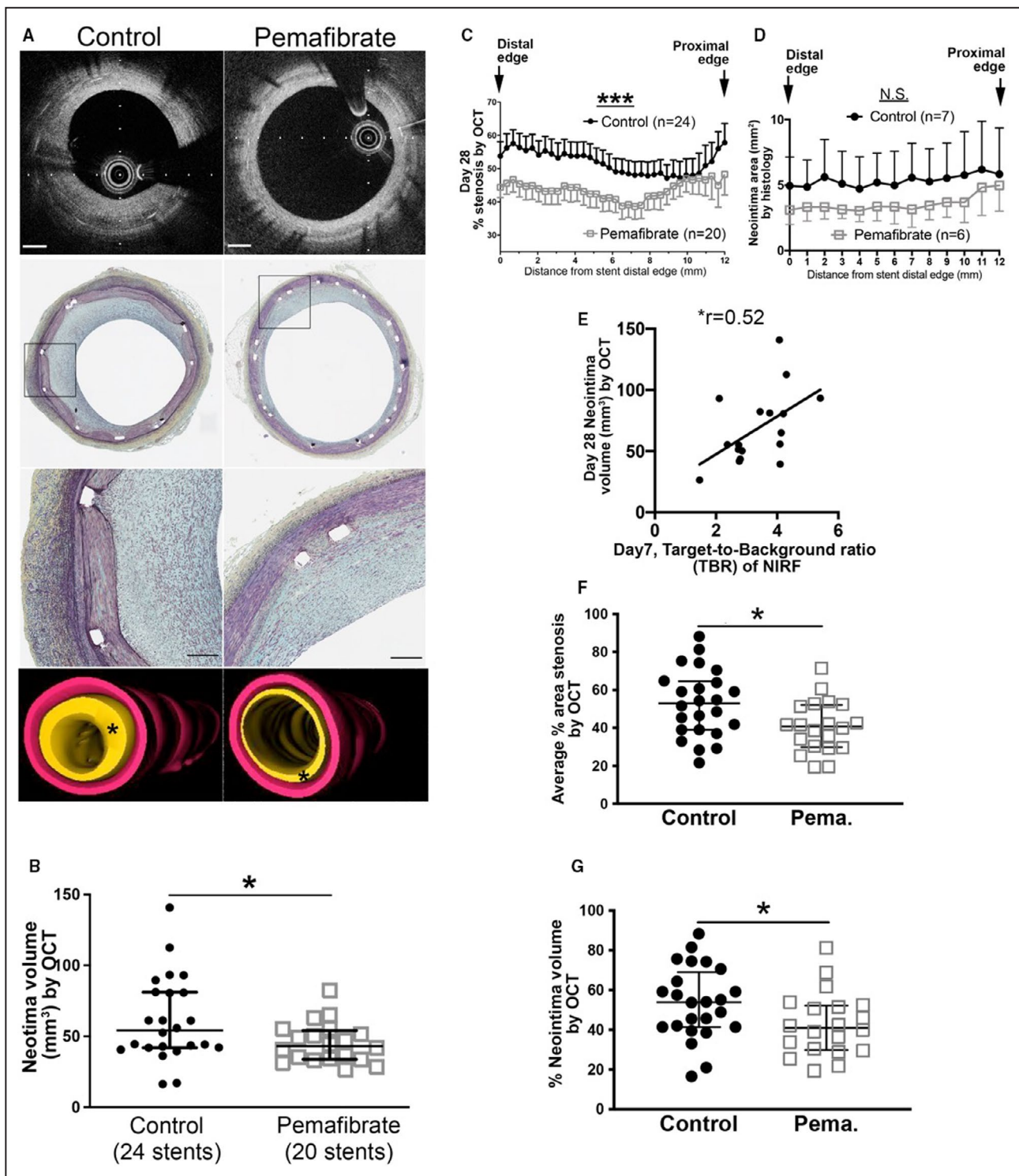
**A**, NIRF signals in the RCA and LAD of a representative control and pemafibrate-treated animal. The day 7 NIRF signal intensity, reflecting inflammatory cathepsin protease activity, was lower in stents of pigs treated with pemafibrate compared with controls. The NIRF signal in nonstented areas was used as the background/reference measurement. A total of 4 representative stents are shown (**left**, control; **right**, pemafibrate [all 2-dimensional NIRF maps equally windowed]). **B**, The NIRF inflammation signal measured as the TBR was significantly lower in pemafibrate-treated animals (9 stents, 3 animals in each group). Each dot indicates 1 stent. Horizontal lines and error bars indicate medians and 25th to 75th percentiles, respectively. LAD indicates left anterior descending coronary artery; NIRF, near-infrared fluorescence; RCA, right coronary artery; and TBR, target-to-background ratio. \* $P < 0.05$ .

correlation was evident between the day 28 peri-strut inflammation or vascular injury score and the neointimal area (Figure S2a and S2c).

### Pemafibrate Enhances the PPAR $\alpha$ Pathway and Suppresses Inflammation and Proliferation in Experimental Stented Arteries and Human Arteries

To examine further the effects of pemafibrate on the in vivo effects of SMC biology, neointima specimens from implanted resected pig coronary artery stents were dissected for mRNA and protein expression studies. The left circumflex coronary artery without stent implantation from the same animal served as a control reference artery. As compared with reference arterial segments, the

intima of stented arteries expressed higher mRNA levels of the proinflammatory cytokine TNF $\alpha$  (tumor necrosis factor- $\alpha$ ; Figure S3a). Pemafibrate treatment reduced stent TNF $\alpha$  expression compared with control stents. Furthermore, the induction of MMP-9 (matrix metalloproteinase 9) in stented intima was nearly abrogated by pemafibrate. Pemafibrate further enhanced the gene expression of PPAR $\alpha$  (consistent with prior studies in endothelial cells and osteoblasts<sup>20,21</sup>) as well as CPT1a (carnitine palmitoyltransferase 1A), a target of the PPAR $\alpha$  pathway, in both the neointima of stented arteries as well as in reference coronary arteries (Figure S2b). In addition, pemafibrate reduced SMC proliferation in human carotid artery culture ex vivo and promoted maturity of human coronary artery SMCs in vitro (Data S1 and Figures S4 and S5).



### Pemafibrate Maintains SMC Differentiation in the Neointima of Pig Coronary Arteries

The combined use of key markers of SMC differentiation such as  $\alpha$ -actin, calponin, smoothelin, and myosin heavy chain helps identify the differentiated state of SMC

during the development of vascular disorders such as atherosclerosis and restenosis.<sup>22–24</sup> The availability of antibodies for such proteins in pigs, however, is limited. We therefore optimized mass spectrometry–assisted proteomics to examine the effects of pemafibrate on the differentiated state of SMC in stented arteries. The expression levels of SMC differentiation markers, such

**Figure 3. Assessment of pemaifibrate on in-stent neointima formation.**

Representative figures of OCT imaging (day 28), histology, and 3-dimensional representation (day 28) in the control and pemaifibrate groups, respectively. **A**, OCT showed that pemaifibrate attenuated in-stent neointima formation. (Scale bars=1 mm.) Movat's pentachrome demonstrated more fibrous, less mucinous (proteoglycan), and lower cell accumulation around stent struts as well as in the adventitia in the pemaifibrate-treated animals. (Scale bars=100  $\mu$ m.) Representative images of 3-dimensional neointima reconstructions in the control and pemaifibrate groups. \*Neointima. **B**, Neointima volume per stent assessed at day 28 was suppressed by pemaifibrate treatment (n=20 stents, 6 animals in the control group; n=24 stents, 7 animals in the pemaifibrate group). **C**, Longitudinal analysis OCT images showed a lower percent luminal stenosis in the pemaifibrate-treated pigs ( $P<0.001$ ), particularly toward the distal stent edge. **D**, Longitudinal analysis of histological images showed similar findings as did the OCT analysis, with lower neointima area across the stent in the pemaifibrate group; however, this trend was not statistically significant ( $P=0.138$ ). Each dot represents the average histology-measured neointimal area at a given stent distance from either control (circles) or pemaifibrate (squares) subjects. **E**, A moderate correlation was found between the early NIRF inflammatory cathepsin protease signal on day 7 and the subsequent neointima volume on day 28 (n=17 stents). Each dot depicts 1 stent. **F**, Mean percentage neointima area stenosis at day 28 derived from OCT images. **G**, Percentage neointima volume per stent at day 28 derived from OCT images. Each dot represents 1 stent with 36 images per stent analyzed every 0.33 mm from the distal stent edge. Horizontal lines and error bars indicate medians and 25th to 75th percentiles, respectively. NIRF indicates near-infrared fluorescence; N.S., not significant; OCT, optical coherence tomography; and Pema., pemaifibrate. \* $P<0.05$ ; \*\*\* $P<0.001$ .

as *CNN1* (calponin 1) and *SMTN* (smoothelin), were higher, and *ACTA2* (SM $\alpha$ -actin) tended to be higher in the pemaifibrate-treated arteries, whereas the expression levels of housekeeping proteins, such as GAPDH,  $\beta$ -actin, and  $\beta$ -tubulin, were similar in the 2 groups (Figure S6). The levels of myosin heavy chain (MYH11), indicative of fully differentiated SMCs, did not differ between groups. These results indicate that PPAR $\alpha$  activation by pemaifibrate may suppress phenotypic modulation of SMCs into the immature stage after stent implantation but do not fully restore the state of mature SMCs.

### Relationship Between Serum Lipid Levels and In Vivo NIRF Inflammation

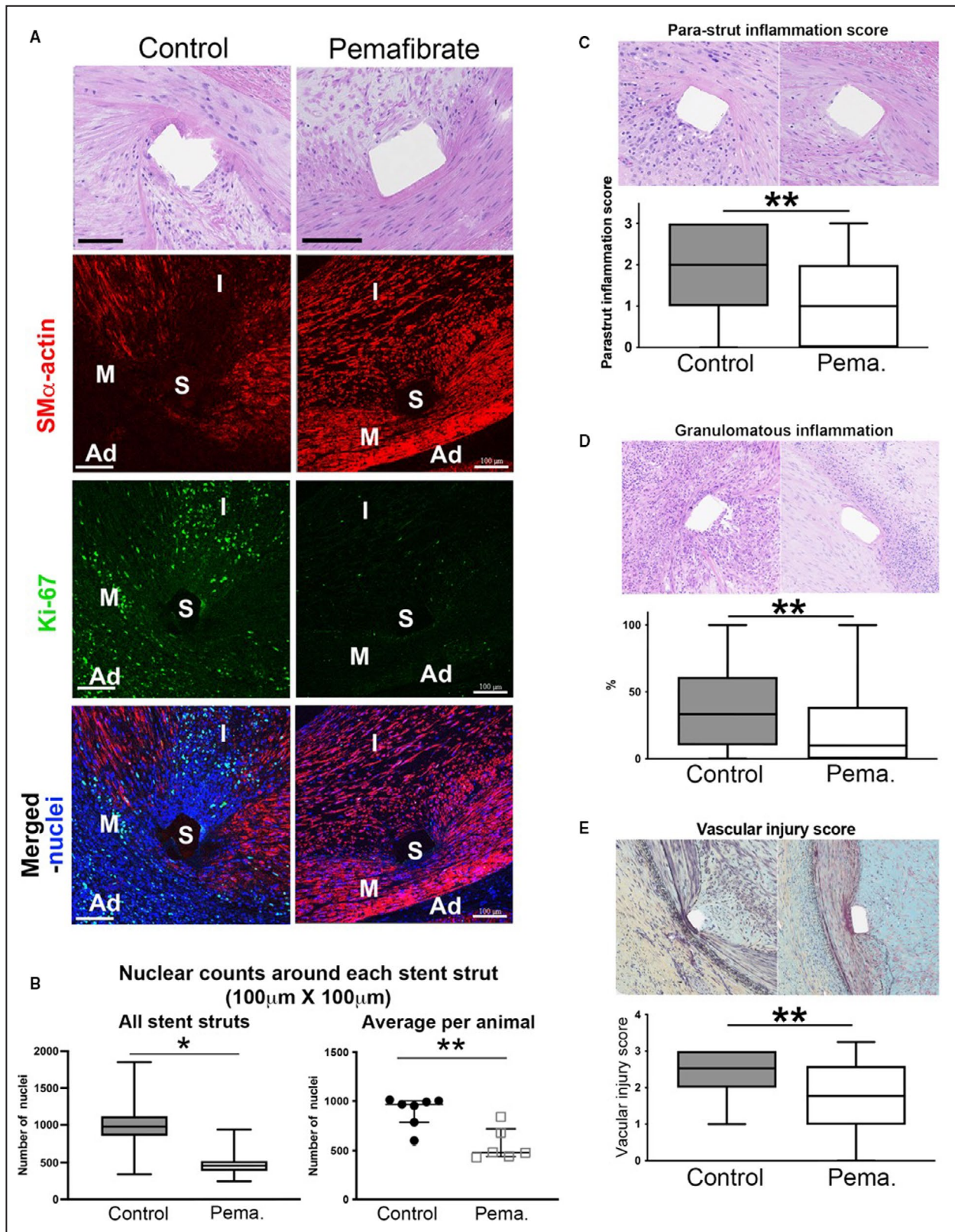
Serum lipids levels were similar between the control and pemaifibrate groups at both day 0 and day 28. Serum high-density lipoprotein cholesterol levels on day 0 and day 28 did not exhibit a significant relationship to the day 7 in vivo NIRF inflammation levels (Figure S7).

## DISCUSSION

This multimodal molecular-microstructural intravascular study demonstrates that the clinically approved potent PPAR $\alpha$  activator pemaifibrate reduces preclinical stent-induced inflammation and restenosis in a preclinical swine model. PPAR $\alpha$  activation in this investigation was achieved through the selective PPAR $\alpha$  activator pemaifibrate, with a potency >1000 times higher than the conventional PPAR $\alpha$  agonist fenofibrate.<sup>9</sup> Our work revealed that pemaifibrate inhibited stent inflammation assessed by high-resolution in vivo NIRF-OCT inflammation imaging and suppression of mRNA neointima inflammatory mediators TNF- $\alpha$  and MMP-9 (matrix metalloproteinase 9). Pemaifibrate further reduced histopathological cell inflammation and proliferation following stent-induced vascular injury. Proteomic analyses of stented arteries, organoid cultures of pig

arteries, and in vitro experiments in human primary SMCs provided additional evidence that pemaifibrate suppressed SMC phenotypic modulation, proinflammatory activation, and proliferation. Overall, these results demonstrate the following: (1) that intravascular molecular-microstructural NIRF-OCT imaging can translationally image the anti-inflammatory effects of new restenosis therapies in vivo and (2) that pemaifibrate may merit evaluation as a new pharmacologic strategy to limit clinical endovascular stent restenosis in patients.

Stent implantation causes local endovascular injury and inflammation, leading to macrophage and SMC activation that promote in-stent restenosis, late neoatherosclerosis, and thrombosis.<sup>6,7,25</sup> In this study, intravascular NIRF-OCT demonstrated reduced in vivo inflammatory cathepsin protease activity and stent neointimal volume in implanted bare metal coronary artery stents of pemaifibrate-treated animals. By reducing activated tissue cathepsins, such as cathepsin S, an important cysteine protease in human atherosclerosis pathobiology that promotes collagenolysis, elastolysis, and facilitates SMC migration,<sup>26–28</sup> pemaifibrate may interrupt a key step in the restenosis process. In addition to suppressing in vivo inflammatory protease activity, pemaifibrate also reduced Ki-67 cellular proliferation and promoted calponin and smoothelin markers of SMC differentiation, effectively decreasing the likelihood of neointima SMC expansion. Although the dose used in the present study does not lower plasma triglyceride levels, we used normolipidemic pigs in this study, and the study time frame was too short to evaluate longer term effects on triglyceride levels. Thus, the effects of pemaifibrate on lesion development, inflammation, and SMC phenotype after stenting were likely mediated by mechanisms independent of the changes in the levels of circulating triglycerides. To further understand mechanisms of reduced neointimal volume induced by pemaifibrate, additional in vitro analyses using primary cultured human SMCs demonstrated



that pemafibrate fostered the mature state of SMC and limited proliferation via the STAT3 (signal transducer and activator of transcription 3) and myocardin

axes. Consistent with prior studies of conventional PPAR $\alpha$  agonists,<sup>29</sup> and with prior pemafibrate studies in atherosclerosis,<sup>30,31</sup> the current results for the first

**Figure 4. The effects of pemafibrate on peri-stent strut cell accumulation and proliferation.**

**A**, Hematoxylin-eosin and immunofluorescence staining of tissues around stent struts on day 28. Cell accumulation and the number of Ki-67+ cells were lower in the pemafibrate group than the control group, whereas SM $\alpha$ -actin expression was higher. **B**, Nuclear count around stent struts per 0.01 mm<sup>2</sup> (100 × 100  $\mu$ m) was significantly lower in the pemafibrate group on a per-strut basis (**left**, N=504 control, N=432 pemafibrate;  $P=0.016$  [box plots indicate medians and 25th–75th percentiles]) as well as on a per-animal basis (**right**, N=7 control, N=6 pemafibrate, 72 stent struts analyzed per animal;  $P=0.008$  [horizontal line and error bars indicate medians and 25th–75th percentiles, respectively]). **C–E**, Histological analysis at day 28 (n=84 sections in the control group, n=72 sections in the pemafibrate group [box plots indicate medians and 25th–75th percentiles]) revealed lower peri-strut inflammation, granulomatous inflammation percentage, and vascular injury scores in the pemafibrate group. (Scale bar=100  $\mu$ m.) Ad indicates adventitia; I, intima; M, media; Pema., pemafibrate; S, stent; and SM $\alpha$ , smooth muscle  $\alpha$ . \* $P<0.05$ , \*\* $P<0.01$ .

time demonstrate that pemafibrate can exert anti-inflammatory and antiproliferative effects in stented arteries, independently of its action on plasma triglycerides, and provide insight into SMC mechanisms underlying the observed pemafibrate-driven reductions in stent restenosis.

Given the importance of inflammation in restenosis and atherosclerosis, there is increasing interest in imaging inflammation in vivo at high resolution in coronary arteries.<sup>32</sup> To enable high-resolution molecular imaging, our laboratories have developed intravascular NIRF imaging platforms for assessing in vivo atheroma and stent pathobiology, including inflammation and fibrin deposition.<sup>16,33,34</sup> Translationally, a NIRF-OCT system has been used in patients with coronary artery disease to detect NIR autofluorescence.<sup>35,36</sup> In addition to ProSense VM110, which has been evaluated clinically (NCT03286062), an analogous cathepsin reporter<sup>37</sup> and the endothelial leakage NIRF agent indocyanine green<sup>14,34</sup> also appear promising for clinical NIRF imaging of coronary artery disease. The current study provides a framework for evaluating whether NIRF imaging of stent inflammation will identify subjects at higher risk for clinical restenosis and for assessing the relationship between inflammation and stent restenosis in patients receiving anti-inflammatory pharmacotherapy.

Although the current study used BMS implantation to efficiently generate higher volumes of neointimal hyperplasia compared with antiproliferative DESs, BMSs currently remain the predominant stent type used during endovascular treatment of PAD, especially given the recent concerns about the use of paclitaxel-coated devices.<sup>38</sup> Moreover, restenosis after endovascular stenting for both femoropopliteal artery and below-the-knee PAD remains a major clinical and costly clinical problem.<sup>39,40</sup> Therefore, if clinically validated, pemafibrate could help improve the outcomes of patients with PAD treated with BMSs. From a coronary standpoint, although further experimental studies are needed to determine the efficacy of pemafibrate on suppressing neointimal hyperplasia in DESs, it is important to note that coronary stent restenosis remains a substantial clinical problem even in the DES era, with rates ranging between 3% to 20%.<sup>41</sup> Coronary

stent restenosis carries increased morbidity and mortality,<sup>1,42</sup> and treatment of refractory restenosis may require coronary artery bypass surgery or invasive intracoronary brachytherapy, which still carries a significant risk of recurrent restenosis.<sup>43</sup> Despite decades of research<sup>44</sup> and the potential for oral cilostazol<sup>45</sup> or colchicine,<sup>46</sup> no oral antirestenosis therapy is yet clinically established.

This study has certain limitations. First, we did not examine the effect of pemafibrate on suppressing DES neointima formation because the higher stent neointima formation afforded by BMSs allowed more efficient restenosis generation; of note, BMSs are routinely used in the treatment of PAD, and the use of BMSs is thus still clinically relevant. Future studies evaluating the effects of pemafibrate on the restenosis following DES implantation are needed, particularly in subjects with coronary artery disease. Second, stent implantation into the normal arteries of male juvenile swines does not fully recapitulate the pathophysiology of restenosis occurring in a milieu of atherosclerosis. Third, although various drugs including those with anti-inflammatory capabilities<sup>47</sup> have demonstrated an antirestenotic effect in preclinical stenting models, similar clinical antirestenotic effects have rarely been reproduced in the patients.<sup>48</sup> Fourth, although the current study design reproduced previous large animal stent studies and indicates significant pemafibrate-induced reductions in stent-induced arterial inflammation and neointima volume on a per-stent basis, as the per-animal comparisons were not significant likely as a result of being underpowered, the NIRF-OCT findings and the overall study findings are considered hypothesis generating. Therefore, although the current study demonstrates promising preclinical antirestenotic effects by pemafibrate, additional validation studies are needed, including those with extended time points, to determine whether pemafibrate could suppress both neointima formation and clinical restenosis rates in patients with PAD and coronary artery disease.

In conclusion, this integrative multimodal intravascular imaging and biological study demonstrates the potential for the novel PPAR $\alpha$  selective activator pemafibrate to reduce preclinical stent in vivo inflammation, cellular proliferation, and neointimal hyperplasia and

therefore may offer a new strategy to reduce clinical endovascular stent restenosis.

## ARTICLE INFORMATION

Received January 12, 2021; accepted June 25, 2021.

### Affiliations

Center for Interdisciplinary Cardiovascular Sciences, Cardiovascular Division (H.I., K.M., C.G., J.D.H., P.C.M., S.A.S., J.M., E.A., M.A.), Center for Excellence in Vascular Biology, Cardiovascular Division (P.L., E.A., M.A.) and Channing Division of Network Medicine (M.A.), Brigham and Women's Hospital, Harvard Medical School, Boston, MA; Department of Cardiovascular Biology and Medicine, Juntendo University Graduate School of Medicine, Tokyo, Japan (H.I.); Cardiovascular Research Center, Cardiology Division (E.A.O., A.M., F.A.J.), Wellman Center for Photomedicine (G.J.U., G.J.T., F.A.J.) and Department of Pathology (G.J.T.), Massachusetts General Hospital, Harvard Medical School, Boston, MA; Cardiology Division, Beth Israel Deaconess Medical Center, Harvard Medical School, Boston, MA (E.A.O.); and Department of Human Pathology, I.M. Sechenov First Moscow State Medical University of the Ministry of Health, Moscow, Russian Federation (E.A.).

### Acknowledgments

We thank Brett Pieper, Jung Choi, Tan H. Pham, Jennifer Wen, and Anna Heewoo Ha for their technical assistance.

### Sources of Funding

This study was supported by research grants from Kowa Company, Ltd, Nagoya, Japan, to Masanori Aikawa and Farouc A. Jaffer, the National Institutes of Health (R01HL126901 and R01HL149302 to Masanori Aikawa; R01HL122388, R01HL137913, and R01HL150538 to Farouc A. Jaffer; K08HL130465 to Eric A. Osborn; R01HL136431 and R01HL147095 to Elena Aikawa; and R01HL080472 to Peter Libby), American Heart Association (18CSA34080399 to Peter Libby), and the RRM Charitable Fund to Peter Libby. The near-infrared fluorescence–optical coherence tomography system was developed in part under R01HL093717 to Guillermo J. Tearney. Kowa Company, Ltd, Nagoya, Japan, provided partial research funding support for this study but was not involved in the study design or data analysis.

### Disclosures

Dr Iwata has received sponsored research from Kowa and Daiichi-Sankyo. Dr Osborn is a consultant for Abbott Vascular and Canon, has served on the scientific advisory board and has equity interest in Dyad Medical, and has received personal fees from Opens Medical. Dr Tearney has received sponsored research from Merck Sharp & Dohme, VivoLight, and Canon; has received royalties and catheter components from Terumo; and has been a consultant for Samsung. Dr Tearney has a financial/fiduciary interest and consults for SpectraWAVE, a company developing an optical coherence tomography–near-infrared fluorescence intracoronary imaging system and catheter. His financial/fiduciary interest was reviewed and is managed by the Massachusetts General Hospital and Partners HealthCare in accordance with their conflict of interest policies. Dr Jaffer has received sponsored research from Kowa, Canon, Siemens, Teleflex, and Shockwave and is a consultant for Boston Scientific, Abbott Vascular, Siemens, Magenta Medical, Asahi Intecc, and IMDS. Dr Jaffer has an equity interest in Intravascular Imaging, Inc. and DurVena. Massachusetts General Hospital has a patent licensing arrangement with Terumo, Canon, and SpectraWAVE; Dr Tearney and Dr Jaffer (Terumo, Canon, SpectraWAVE) have the right to receive royalties. Dr Aikawa has received sponsored research from Kowa, Pfizer, and Sanofi. Dr Libby has been an unpaid consultant to or is involved in clinical trials for Amgen, AstraZeneca, Esperion Therapeutics, Ionis Pharmaceuticals, Kowa Pharmaceuticals, Novartis, Pfizer, Sanofi-Regeneron, and XBiotech, Inc. and has been a member of scientific advisory boards for Amgen, Athera Biotechnologies, Corvidia Therapeutics, DalCor Pharmaceuticals, IFM Therapeutics, Kowa Pharmaceuticals, Olatec Therapeutics, Medimmune, and Novartis, and his laboratory has received research funding in the past 2 years from Novartis.

### Supplementary Material

Data S1  
Tables S1–S3

Figures S1–S7  
References 49–60

## REFERENCES

- Cassese S, Byrne RA, Schulz S, Hoppman P, Kreutzer J, Feuchtenberger A, Ibrahim T, Ott I, Fusaro M, Schunkert H, et al. Prognostic role of restenosis in 10 004 patients undergoing routine control angiography after coronary stenting. *Eur Heart J*. 2015;36:94–99. DOI: 10.1093/eurheartj/ehu383.
- Shlofmitz E, Iantorno M, Waksman R. Restenosis of drug-eluting stents. *Circ Cardiovasc Interv*. 2019;12:e007023. DOI: 10.1161/CIRCINTERVENTIONS.118.007023.
- Kubo T, Akasaka T. Continuous development of neoatherosclerosis beyond a decade after drug-eluting stent implantation. *EuroIntervention*. 2018;14:e1255–e1257. DOI: 10.4244/EIJV14H12A226.
- Nakazawa G, Otsuka F, Nakano M, Vorpahl M, Yazdani SK, Ladich E, Kolodgie FD, Finn AV, Virmani R. The pathology of neoatherosclerosis in human coronary implants bare-metal and drug-eluting stents. *J Am Coll Cardiol*. 2011;57:1314–1322. DOI: 10.1016/j.jacc.2011.01.011.
- Guerra E, Byrne RA, Kastrati A. Pharmacological inhibition of coronary restenosis: systemic and local approaches. *Expert Opin Pharmacother*. 2014;15:2155–2171. DOI: 10.1517/14656566.2014.948844.
- Libby P, Schwartz D, Brogi E, Tanaka H, Clinton SK. A cascade model for restenosis. A special case of atherosclerosis progression. *Circulation*. 1992;86:1147–52.
- Aikawa M, Manabe I, Chester A, Aikawa E. Cardiovascular Inflammation. *Int J Inflamm*. 2012;2012:1–2. DOI: 10.1155/2012/904608. DOI: 10.1155/2012/904608.
- Ishibashi S, Yamashita S, Arai H, Araki E, Yokote K, Suganami H, Fruchart JC, Kodama T, Group KS. Effects of K-877, a novel selective PPARalpha modulator (SPPARMalpha), in dyslipidaemic patients: A randomized, double blind, active- and placebo-controlled, phase 2 trial. *Atherosclerosis*. 2016;249:36–43.
- Fruchart JC. Selective peroxisome proliferator-activated receptor alpha modulators (SPPARMalpha): the next generation of peroxisome proliferator-activated receptor alpha-agonists. *Cardiovasc Diabetol*. 2013;12:82.
- Marx N, Sukhova GK, Collins T, Libby P, Plutzky J. PPARalpha activators inhibit cytokine-induced vascular cell adhesion molecule-1 expression in human endothelial cells. *Circulation*. 1999;99:3125–3131.
- Effect of fenofibrate on progression of coronary-artery disease in type 2 diabetes: the Diabetes Atherosclerosis Intervention Study, a randomised study [published correction appears in *Lancet* 2001 Jun;357(9271):1890]. *Lancet* 2001;357:905–910.
- Corti R, Osende J, Hutter R, Viles-Gonzalez JF, Zafar U, Valdivieso C, Mizsei G, Fallon JT, Fuster V, Badimon JJ. Fenofibrate induces plaque regression in hypercholesterolemic atherosclerotic rabbits: in vivo demonstration by high-resolution MRI. *Atherosclerosis*. 2007;190:106–113. DOI: 10.1016/j.atherosclerosis.2006.02.036.
- Yoo H, Kim JW, Shishkov M, Namati E, Morse T, Shubochkin R, McCarthy JR, Ntziachristos V, Bouma BE, Jaffer FA, et al. Intra-arterial catheter for simultaneous microstructural and molecular imaging in vivo. *Nat Med*. 2011;17:1680–1684. DOI: 10.1038/nm.2555.
- Verjans JW, Osborn EA, Ughi GJ, Calfon Press MA, Hamidi E, Antoniadis AP, Papafaklis MI, Conrad MF, Libby P, Stone PH, et al. Targeted near-infrared fluorescence imaging of atherosclerosis: clinical and intracoronary evaluation of indocyanine green. *JACC Cardiovasc Imaging*. 2016;9:1087–1095.
- Hara T, Ughi GJ, McCarthy JR, Erdem SS, Mauskopf A, Lyon SC, Fard AM, Edelman ER, Tearney GJ, Jaffer FA. Intravascular fibrin molecular imaging improves the detection of unhealed stents assessed by optical coherence tomography in vivo. *Eur Heart J*. 2017;38:447–455.
- Bozhko D, Osborn EA, Rosenthal A, Verjans JW, Hara T, Kellnberger S, Wissmeyer G, Ovsepian SV, McCarthy JR, Mauskopf A, et al. Quantitative intravascular biological fluorescence-ultrasound imaging of coronary and peripheral arteries in vivo. *Eur Heart J Cardiovasc Imaging*. 2017;18:1253–1261. DOI: 10.1093/ehjci/jew222.
- Calfon Press MA, Mallas G, Rosenthal A, Hara T, Mauskopf A, Nudelman RN, Sheehy A, Polyakov IV, Kolodgie F, Virmani R, et al.

- Everolimus-eluting stents stabilize plaque inflammation in vivo: assessment by intravascular fluorescence molecular imaging. *Eur Heart J Cardiovasc Imaging*. 2017;18:510–518. DOI: 10.1093/ehjci/jew228.
18. Wiegand BR, Pompeu D, Thiel-Cooper RL, Cunnick JE, Parrish FC Jr. Immune response and blood chemistry of pigs fed conjugated linoleic acid. *J Anim Sci*. 2011;99:1588–1594.
  19. Rustemeyer SM, Lamberson WR, Ledoux DR, Wells K, Austin KJ, Cammack KM. Effects of dietary aflatoxin on the hepatic expression of apoptosis genes in growing barrows. *J Anim Sci*. 2011;99:916–925.
  20. Inoue I, Shino K, Noji S, Awata T, Katayama S. Expression of peroxisome proliferator-activated receptor alpha (PPAR alpha) in primary cultures of human vascular endothelial cells. *Biochem Biophys Res Commun*. 1998;246:370–374.
  21. Kim YH, Jang WG, Oh SH, Kim JW, Lee MN, Song JH, Yang JW, Zang Y, Koh JT. Fenofibrate induces PPARalpha and BMP2 expression to stimulate osteoblast differentiation. *Biochem Biophys Res Commun*. 2019;520:459–465.
  22. Aikawa M, Sakomura Y, Ueda M, Kimura K, Manabe I, Ishiwata S, Komiya N, Yamaguchi H, Yazaki Y, Nagai R. Redifferentiation of smooth muscle cells after coronary angioplasty determined via myosin heavy chain expression. *Circulation*. 1997;96:82–90. DOI: 10.1161/01.CIR.96.1.82.
  23. Aikawa M, Sivam PN, Kuro-o M, Kimura K, Nakahara K, Takewaki S, Ueda M, Yamaguchi H, Yazaki Y, Periasamy M, et al. Human smooth muscle myosin heavy chain isoforms as molecular markers for vascular development and atherosclerosis. *Circ Res*. 1993;73:1000–1012. DOI: 10.1161/01.RES.73.6.1000.
  24. Iwata H, Manabe I, Fujiu K, Yamamoto T, Takeda N, Eguchi K, Furuya A, Kuro-o M, Sata M, Nagai R. Bone marrow-derived cells contribute to vascular inflammation but do not differentiate into smooth muscle cell lineages. *Circulation*. 2010;122:2048–2057. DOI: 10.1161/CIRCULATIONAHA.110.965202.
  25. Inoue T, Croce K, Morooka T, Sakuma M, Node K, Simon DI. Vascular inflammation and repair: implications for re-endothelialization, restenosis, and stent thrombosis. *JACC Cardiovasc Interv*. 2011;4:1057–1066. DOI: 10.1016/j.jcin.2011.05.025.
  26. Cheng XW, Kuzuya M, Nakamura K, Di Q, Liu Z, Sasaki T, Kanda S, Jin H, Shi GP, Murohara T, et al. Localization of cysteine protease, cathepsin S, to the surface of vascular smooth muscle cells by association with integrin alpha5beta3. *Am J Pathol*. 2006;168:685–694.
  27. Wu H, Du Q, Dai Q, Ge J, Cheng X. Cysteine protease cathepsins in atherosclerotic cardiovascular diseases. *J Atheroscler Thromb*. 2018;25:111–123. DOI: 10.5551/jat.RV17016.
  28. Marx SO, Totary-Jain H, Marks AR. Vascular smooth muscle cell proliferation in restenosis. *Circ Cardiovasc Interv*. 2011;4:104–111. DOI: 10.1161/CIRCINTERVENTIONS.110.957332.
  29. Kasai T, Miyauchi K, Yokoyama T, Aihara K, Daida H. Efficacy of peroxisome proliferative activated receptor (PPAR)-alpha ligands, fenofibrate, on intimal hyperplasia and constrictive remodeling after coronary angioplasty in porcine models. *Atherosclerosis*. 2006;188:274–280.
  30. Konishi H, Miyauchi K, Onishi A, Suzuki S, Fuchimoto D, Shitara J, Endo H, Wada H, Doi S, Naito R, et al. Effect of pemafibrate (K-877), a novel selective peroxisome proliferator-activated receptor alpha modular (SPPARalpha), in atherosclerosis model using low density lipoprotein receptor knock-out swine with balloon injury. *PLoS One*. 2020;15:e0241195.
  31. Hennuyer N, Duplan I, Paquet C, Vanhoutte J, Woitrain E, Touche V, Colin S, Vallez E, Lestavel S, Lefebvre P, et al. The novel selective PPARalpha modulator (SPPARalpha) pemafibrate improves dyslipidemia, enhances reverse cholesterol transport and decreases inflammation and atherosclerosis. *Atherosclerosis*. 2016;249:200–208.
  32. Osborn EA, Jaffer FA. The advancing clinical impact of molecular imaging in CVD. *JACC Cardiovasc Imaging*. 2013;6:1327–1341. DOI: 10.1016/j.jcmg.2013.09.014.
  33. Hara T, Bhayana B, Thompson B, Kessinger CW, Khatri A, McCarthy JR, Weissleder R, Lin CP, Tearney GJ, Jaffer FA. Molecular imaging of fibrin deposition in deep vein thrombosis using fibrin-targeted near-infrared fluorescence. *JACC Cardiovasc Imaging*. 2012;5:607–615. DOI: 10.1016/j.jcmg.2012.01.017.
  34. Vinegoni C, Botnaru I, Aikawa E, Calfon MA, Iwamoto Y, Folco EJ, Ntziachristos V, Weissleder R, Libby P, Jaffer FA. Indocyanine green enables near-infrared fluorescence imaging of lipid-rich, inflamed atherosclerotic plaques. *Sci Transl Med*. 2011;3(84):84ra45. DOI: 10.1126/scitranslmed.3001577.
  35. Htun NM, Chen YC, Lim B, Schiller T, Maghzal GJ, Huang AL, Elgass KD, Rivera J, Schneider HG, Wood BR, et al. Near-infrared autofluorescence induced by intraplaque hemorrhage and heme degradation as marker for high-risk atherosclerotic plaques. *Nat Commun*. 2017;8:75. DOI: 10.1038/s41467-017-00138-x.
  36. Ughi GJ, Wang H, Gerbaud E, Gardecki JA, Fard AM, Hamidi E, Vacas-Jacques P, Rosenberg M, Jaffer FA, Tearney GJ. Clinical characterization of coronary atherosclerosis with dual-modality OCT and near-infrared autofluorescence imaging. *JACC Cardiovasc Imaging*. 2016;9:1304–1314.
  37. Whitley MJ, Cardona DM, Lazarides AL, Spasojevic I, Ferrer JM, Cahill J, Lee C-L, Snuderl M, Blazer DG, Hwang ES, et al. A mouse-human phase 1 co-clinical trial of a protease-activated fluorescent probe for imaging cancer. *Sci Transl Med*. 2016;8(320):320ra4. DOI: 10.1126/scitranslmed.aad0293.
  38. Katsanos K, Spiliopoulos S, Kitrou P, Krokidis M, Karnabatidis D. Risk of death following application of paclitaxel-coated balloons and stents in the femoropopliteal artery of the leg: a systematic review and meta-analysis of randomized controlled trials. *J Am Heart Assoc*. 2018;7:e011245. DOI: 10.1161/JAHA.118.011245.
  39. Dake MD, Ansel GM, Jaff MR, Ohki T, Saxon RR, Smouse HB, Machan LS, Snyder SA, O'Leary EE, Ragheb AO, et al. Durable clinical effectiveness with paclitaxel-eluting stents in the femoropopliteal artery: 5-year results of the Zilver PTX randomized trial. *Circulation*. 2016;133:1472–1483. discussion 1483. DOI: 10.1161/CIRCULATIONAHA.115.016900.
  40. Goldsweig AM, Aronow HD. Novel strategies to reduce femoropopliteal restenosis: Low-dose paclitaxel-coated balloons and paclitaxel-coated balloons plus stenting. *Circulation*. 2017;135:2237–2240. DOI: 10.1161/CIRCULATIONAHA.117.028308.
  41. Dangas GD, Claessen BE, Caixeta A, Sanidas EA, Mintz GS, Mehran R. In-stent restenosis in the drug-eluting stent era. *J Am Coll Cardiol*. 2010;56:1897–1907. DOI: 10.1016/j.jacc.2010.07.028.
  42. Waksman R, Steinvil A. In-stent restenosis? the raiders of the magic remedy. *Circ Cardiovasc Interv*. 2016;9. DOI: 10.1161/CIRCINTERVENTIONS.116.004150.
  43. Mangione FM, Jatene T, Badr Eslam R, Bergmark BA, Gallagher JR, Shah PB, Mauri L, Leopold JA, Sobieszczyk PS, Faxon DP, et al. Usefulness of intracoronary brachytherapy for patients with resistant drug-eluting stent restenosis. *Am J Cardiol*. 2017;120:369–373. DOI: 10.1016/j.amjcard.2017.04.036.
  44. Byrne RA, Joner M, Kastrati A. Stent thrombosis and restenosis: what have we learned and where are we going? The Andreas Gruntzig lecture ESC 2014. *Eur Heart J*. 2015;36:3320–3331.
  45. Miura T, Miyashita Y, Soga Y, Hozawa K, Dojiri T, Ikeda U, Kuwahara K, Di S. Drug-eluting versus bare-metal stent implantation with or without cilostazol in the treatment of the superficial femoral artery. *Circ Cardiovasc Interv*. 2018;11:e006564. DOI: 10.1161/CIRCINTERVENTIONS.118.006564.
  46. Deffereos S, Giannopoulos G, Raisakis K, Kossyvakis C, Kaoukis A, Panagopoulou V, Driva M, Hahalas G, Pyrgakis V, Alexopoulos D, et al. Colchicine treatment for the prevention of bare-metal stent restenosis in diabetic patients. *J Am Coll Cardiol*. 2013;61:1679–1685. DOI: 10.1016/j.jacc.2013.01.055.
  47. Ialenti A, Grassia G, Gordon P, Maddaluno M, Di Lauro MV, Baker AH, Guglielmotti A, Colombo A, Biondi G, Kennedy S, et al. Inhibition of in-stent restenosis by oral administration of bindarit in porcine coronary arteries. *Arterioscler Thromb Vasc Biol*. 2011;31:2448–2454. DOI: 10.1161/ATVBAHA.111.230078.
  48. Colombo A, Basavarajiah S, Limbruno U, Picchi A, Lettieri C, Valgimigli M, Sciahbasi A, Prati F, Calabresi M, Pierucci D, et al. A double-blind randomized study to evaluate the efficacy and safety of bindarit in preventing coronary stent restenosis. *EuroIntervention*. 2016;12:e1385–e1394. DOI: 10.4244/EIJY15M12\_03.
  49. Ughi GJ, Verjans J, Fard AM, Wang H, Osborn E, Hara T, Mauskopf A, Jaffer FA, Tearney GJ. Dual modality intravascular optical coherence tomography (OCT) and near-infrared fluorescence (NIRF) imaging: a fully automated algorithm for the distance-calibration of NIRF signal intensity for quantitative molecular imaging. *Int J Cardiovasc Imaging*. 2015;31:259–268. DOI: 10.1007/s10554-014-0556-z.
  50. Schneider CA, Rasband WS, Eliceiri KW. NIH Image to ImageJ: 25 years of image analysis. *Nat Methods*. 2012;9:671–675. DOI: 10.1038/nmeth.2089.
  51. Mintz GS, Nissen SE, Anderson WD, Bailey SR, Erbel R, Fitzgerald PJ, Pinto FJ, Rosenfield K, Siegel RJ, Tuzcu EM, et al. American college

- of cardiology clinical expert consensus document on standards for acquisition, measurement and reporting of intravascular ultrasound studies (IVUS). A report of the American college of cardiology task force on clinical expert consensus documents. *J Am Coll Cardiol*. 2001;37:1478–1492.
52. Tearney GJ, Regar E, Akasaka T, Adriaenssens T, Barlis P, Bezerra HG, Bouma B, Bruining N, Cho J-M, Chowdhary S, et al. Consensus standards for acquisition, measurement, and reporting of intravascular optical coherence tomography studies: a report from the International Working Group for Intravascular Optical Coherence Tomography Standardization and Validation. *J Am Coll Cardiol*. 2012;59:1058–1072. DOI: 10.1016/j.jacc.2011.09.079.
  53. Schwartz RS, Huber KC, Murphy JG, Edwards WD, Camrud AR, Vlietstra RE, Holmes DR. Restenosis and the proportional neointimal response to coronary artery injury: results in a porcine model. *J Am Coll Cardiol*. 1992;19:267–274. DOI: 10.1016/0735-1097(92)90476-4.
  54. Wilson GJ, Nakazawa G, Schwartz RS, Huibregtse B, Poff B, Herbst TJ, Baim DS, Virmani R. Comparison of inflammatory response after implantation of sirolimus- and paclitaxel-eluting stents in porcine coronary arteries. *Circulation*. 2009;120(141–9):1–2.
  55. Itou T, Maldonado N, Yamada I, Goettsch C, Matsumoto J, Aikawa M, Singh S, Aikawa E. Cystathionine gamma-lyase accelerates osteoclast differentiation: identification of a novel regulator of osteoclastogenesis by proteomic analysis. *Arterioscler Thromb Vasc Biol*. 2014;34:626–634.
  56. Eng J, McCormack A, Yates J. An approach to correlate tandem mass spectral data of peptides with amino acid sequences in a protein database. *Am Soc Mass Spectrom*. 1994;5:976–989. DOI: 10.1016/1044-0305(94)80016-2.
  57. Käll L, Canterbury J, Weston J, Noble W, MacCoss M. Semi-supervised learning for peptide identification from shotgun proteomics datasets. *Nat Methods*. 2007;4:923–925. DOI: 10.1038/nmeth1113.
  58. Elias JE, Gygi SP. Target-decoy search strategy for increased confidence in large-scale protein identifications by mass spectrometry. *Nat Methods*. 2007;4:207–214. DOI: 10.1038/nmeth1019.
  59. Shimamoto Y, Kitamura H, Niimi K, Yoshikawa Y, Hoshi F, Ishizuka M, Takahashi E. Selection of suitable reference genes for mRNA quantification studies using common marmoset tissues. *Mol Biol Rep*. 2013;40:6747–6755. DOI: 10.1007/s11033-013-2791-0.
  60. Liao XH, Wang N, Zhao DW, Zheng DL, Zheng L, Xing WJ, Ma WJ, Bao LY, Dong J, Zhang TC. STAT3 protein regulates vascular smooth muscle cell phenotypic switch by interaction with myocardin. *J Biol Chem*. 2015;290:19641–19652. DOI: 10.1074/jbc.M114.630111.

# **Supplemental Material**

## **Data S1.**

### **Supplemental Methods**

#### **Coronary stent implantation**

Anesthesia was induced by intramuscular injection of Telazol (4.4 mg/kg) and Xylazine (2.2 mg/kg), followed by intubation and mechanical ventilation under sustained maintenance isoflurane inhalation (1-3% isoflurane in O<sub>2</sub> at 3 L/min). After percutaneous or surgical insertion of a 7F sheath (Terumo) into the femoral or carotid artery, heparin was administered (100 Units/kg IV). X-ray coronary angiography was then performed in orthogonal views with manual injections of iodinated contrast media (iopromide, 370 mg/ml, McKesson). A 7F Judkins right or hockey stick guiding catheter (Cordis) was used to engage with the RCA or LCA, respectively. An 0.014-inch guidewire (Prowater, Asahi or Balance Middleweight Universal, Cordis) was inserted into the distal coronary artery. Coronary IVUS images were then acquired by automated 0.5 mm/s pullback with a 40 MHz clinical catheter system (Atlantis SR Pro, Galaxy2; Boston Scientific; Natick, MA). Using IVUS image guidance to determine the proximal and distal reference vessel diameters, 1 or 2 bare metal stents (3.5 x 12 mm, Multi-Link Vision, Abbott Vascular) were implanted into the mid segment of each artery at 12-16 atm. Post-stent IVUS imaging was performed to confirm stent implantation sizing, with use of appropriately sized post-dilatation balloons as needed to achieve a desired 1.3:1 stent:vessel lumen size ratio.

#### **Administration of medications and laboratory testing**

For the duration of the entire protocol (35 days), pigs received aspirin (81 mg/day orally, McKesson), clopidogrel (75 mg/day orally, McKesson), and either pemafibrate (1 mg/kg/day orally, Kowa, Nagoya, Japan) or PBS, in the control group. Pemafibrate was mixed with each animal's daily food preparation allowing for confirmation of drug ingestion. Amiodarone (400 mg daily) was orally administered for three days before and after stent implantation (for a total duration of 7 days) to prevent catheterization or PCI-induced ventricular arrhythmias. Serum lipids and hepatic enzymes were measured at days 0, 7, and 28 after stenting (Automatic Analyzer Labocpect0003, Hitachi High-Technologies Corporation, Tokyo, Japan, and LC-20A system, Shimadzu Corporation, Kyoto, Japan).

#### **NIRF-OCT imaging system**

The NIRF-OCT imaging system and catheter used in this study have been previously described<sup>13-15,36</sup>. Following blood displacement obtained using a manual injection of contrast media through the coronary guiding catheter, the NIRF-OCT imaging system acquires

simultaneous, co-registered NIRF and OCT data at a speed up to 25 frames per second and a pullback velocity of up to 40 mm/s, while the frame rate was 100 in the standalone OCT imaging system. Quantitative fluorescence data are obtained as previously described<sup>49</sup>. Two-dimensional (2D) fluorescence maps are subsequently generated and display the NIRF signal intensity distribution for an entire vessel segment. The vertical axis corresponds to the acquisition angle (i.e., 0 to 360 degree) and the horizontal axis to the vessel longitudinal distance. The approximate axial and lateral resolution for the OCT images are 10-15  $\mu\text{m}$  and 30-60  $\mu\text{m}$ , respectively, and the system signal-to-noise-ratio (SNR) quantified to be > 110 dB. The NIRF data are acquired with a lateral resolution of approximately 100-200  $\mu\text{m}$ , and an SNR > 50 dB for a concentration of 100 nM of the ProSense VM110 imaging agent.

### **Optical coherence tomography (OCT)**

Manual segmentation of OCT images was performed using ImageJ software (National Institute of Health, Bethesda, MD)<sup>50</sup> according to expert consensus recommendations<sup>51,52</sup>. For each OCT pullback at day 7 and day 28, image slices were anatomically co-registered according to the distance from the distal stent edge visualized by OCT. The stent and lumen cross-sectional area (CSA) of each slice within the stent then was measured every 0.33 mm for each OCT pullback. All cross-sectional slices obtained were analyzed and included in the image analysis results. Neointima CSA per slice was calculated as the difference between the stent and lumen CSA, with images analyzed every 0.33 mm across each 12 mm stent (total 36 image slices per stent). The neointima and stent volume ( $\text{mm}^3$ ) per stent was defined by multiplying the summed neointima area or stent area ( $\text{mm}^2$ ) by 0.33 mm (image slice thickness), respectively. The mean %-area stenosis was defined as the average of the %-area stenosis across all slices. The %-neointima volume was defined as the neointima volume ( $\text{mm}^3$ ) divided by the stent volume ( $\text{mm}^3$ ).

### **Near-infrared fluorescence (NIRF)-OCT image analysis**

Regions-of-interest (ROIs) in the stented (target) and the non-stented adjacent (background) vessel were traced manually based on the visual assessment of stent borders. Target-to-background ratios (TBRs) were calculated by dividing the mean ROI signals of the target and background region in ImageJ. NIRF quantitative data were obtained using a previously described automated distance compensation algorithm that corrects the NIRF signal intensity according to the distance between the intravascular imaging catheter and the vessel wall on co-registered OCT images<sup>52</sup>.

### **3-Dimensional image reconstructions**

Using the intracoronary OCT data, a 3-dimensional (3D) reconstruction of the stent and intima was built using vertices of contours of manually traced stent area and lumen area in the cross-sectional images. A vertex set obtained from each slice was piled sequentially and a minimal set of triangles created from the vertices to make a Standard Triangulated Language (STL) file in ImageJ rendered into a 3D model.

### **Histologic examination**

Stented arteries (one stent per animal) were fixed in 4% paraformaldehyde overnight at 4°C prior to commercial processing for histology staining by embedding in MVM resin and saw and grinding sectioning every 0.5mm. From each level, Hematoxylin and Eosin (H&E) and Movat's Pentachrome staining were performed (CBSET, Lexington, MA). The peri-strut inflammation, granulomatous inflammation, and vascular injury scores were assessed using H&E and Movat's pentachrome stained sections, respectively, as previously described<sup>53, 54</sup>.

### **Immunofluorescence**

For immunofluorescence staining, resin was removed by the following protocol: 1 hour xylene, 1 hour 2-methoxyethylacetate, 10 min acetone, followed by decreasing ethanol from 100% to 75%. Next, endogenous peroxidases were quenched in 3% H<sub>2</sub>O<sub>2</sub> for 20 min. Antigen unmasking was performed utilized citrate buffer at pH 6.0 in a pressure cooker. After blocking in 4% of appropriate serum, sections were incubated with a proliferation-targeted Ki-67 primary antibody (1:100; Abcam 15580) for 2 hours, followed by streptavidin-coupled Alexa Fluor 488 secondary antibody (Life Technologies) for 45 minutes. Next, a second primary antibody, SM $\alpha$ -actin-Cy3 (clone 1A4, 1:200; Sigma Aldrich) was applied overnight at 4°C to enable multichannel fluorescence imaging. Sections were washed in PBS and embedded in mounting medium containing DAPI (Vector Laboratories). Slides were examined using a confocal microscope A1 (Nikon). SM $\alpha$ -actin and Ki-67 data were captured centered on the peri-strut area, as defined by the absence of tissue in the stent strut zones on histological sections. All images were processed with Elements 3.20 software (Nikon).

### **Protein isolation and proteomics analysis**

The intima of stented right coronary artery segments (n=3 in each group) were excised and put into RIPA buffer on ice. Tissues were homogenized using a Procellys 24 tissue homogenizer. The resultant supernatant was immediately stored at -80°C. In each sample, 15  $\mu$ g of protein was subjected to further proteolysis followed by liquid chromatography tandem mass spectrometry (LS/-MS/LS).

## **Proteolysis**

Proteolysis (Trypsin, MS grade Promega) was completed using the in-solution urea+ RapiGest (Waters) strategy detailed<sup>55</sup>. The tryptic peptides were desalted using Oasis Hlb 1cc (10 mg) columns (Waters, USA), and dried with a tabletop speed vacuum (SPD1010, Thermo Fisher Scientific, USA). The peptides were resuspended in 40  $\mu$ l of 5% mass spectrometry grade acetonitrile (Thermo Fisher Scientific, USA) and 5% formic acid (Sigma-Aldrich, USA).

## **Liquid chromatography tandem mass spectrometry (LC-MS/MS)**

The peptides were analyzed using the Q Exactive (classic model) mass spectrometer fronted with a Nanospray FLEX ion source, coupled to an Easy-nLC1000 HPLC pump (Thermo Fisher Scientific). The peptides were subjected to a dual column set-up: an Acclaim PepMap RSLC C18 trap column, 75  $\mu$ m X 20 mm; and an Acclaim PepMap RSLC C18 analytical column 75  $\mu$ m X 250 mm (Thermo Fisher Scientific). All reagents were MS-grade. The MS1 scan was set to 140 K resolution, and the top 10 precursor ions (within a scan range of 380-1500 m/z) were subjected to higher energy collision induced dissociation (HCD, collision energy 25% (+/- 10%)), isolation width 1.6 m/z, dynamic exclusion enabled (20 seconds), and resolution set to 17.5 K for peptide sequencing (MS/MS).

The LC-MS/MS data were queried against the Pig UniProt database (August 1, 2014) using the SEQUEST search algorithm<sup>56</sup>, via the Proteome Discoverer (PD) Package (version 1.3, Thermo Fisher Scientific), using a 10 ppm tolerance window in the MS1 search space, and a 0.02 Da fragment tolerance window for HCD. The peptide false discovery rate (FDR) was calculated using Percolator provided by PD: the FDR was determined based on the number of MS/MS spectral hits<sup>57,58</sup>. Peptides were filtered based on a 1% FDR. Peptides assigned to a given protein group, and not present in any other protein group, were considered as unique. Consequently, each protein group was represented by a single master protein (PD Grouping feature). Master proteins with two or more unique peptides were used for ratio quantification. Quantification was done using the total peptide spectrum matches (PSMs) per protein.

## **Quantitative real-time PCR**

Total RNA from coronary artery intima and media, and from primary cultured human coronary artery smooth muscle cells, was isolated using TriZol (Life Technologies). Reverse transcription was performed using the QuantiTect Reverse Transcription Kit (Qiagen). mRNA expression was determined by TaqMan-based real-time PCR reactions (Life

Technologies) in ABI 7900 HT fast real time PCR systems (Applied Biosystems). The following TaqMan probes were used – pig tissues: TNF: Ss03391316\_g1, MMP9: Ss03392100\_m1, PPARA: Ss03380164\_u1, CPT1A: Ss03373367\_m1, RPLP0: Ss03389091\_m1; cells: CNN1: Hs00154543\_m1, ACTA2: Hs00426835\_g1. The expression levels were normalized to RPLP0<sup>59</sup>. Results were calculated using the Delta-Delta Ct method and presented as arbitrary units.

### **Ex vivo carotid artery ring organoid culture**

Freshly resected uninjured carotid arteries from control pigs (did not receive pemaifibrate) were cut into 0.1 cm thick rings and incubated in DMEM (10% FBS, 1% PS) for 24 hours. Then, the medium was changed to DMEM (0.1% FBS) with or without 10  $\mu$ M pemaifibrate for 2 hours as preincubation. Rings were then incubated with 10 nM PDGF for 24 hours. Afterwards, artery rings were embedded in OCT compound stored at -80°C, and 7- $\mu$ m thickness cryosections fixed in 4% PFA and stained with Ki-67 Alexa-Fluor 488, SM $\alpha$ -actin-Cy3, and DAPI for multichannel confocal fluorescence microscopy as described above. Signals of 4 fields in 3 levels with 0.1 mm interval were counted by using ImageJ software.

### **Primary smooth muscle cell (SMC) culture**

Human coronary artery SMCs (HCASMCs) were obtained from Promocell (C-12511) and cultured SMC growth medium 2 (Promocell, C-22262). For evaluating SMC differentiation marker genes and protein expression, HCASMCs (semi-confluent) were treated with pemaifibrate (10  $\mu$ M) before stimulation with PDGF-BB (10 ng/ml, Prospec, CYT-501) for 16 hours. For cell proliferation assays, HCASMCs were seeded on 24 well plates in  $4 \times 10^3$  cells/well for overnight incubation. Afterwards, pemaifibrate (1-10  $\mu$ M) and fenofibric acid (100  $\mu$ M) were supplemented at 1 hour prior to PDGF-BB stimulation (10 ng/ml) for 12 hours.

### **Cell proliferation assay**

BrdU incorporation analysis was performed on HCASMC primary cultures using a BrdU Cell Proliferation Assay Kit (Cell Signaling Technology, 6813S). Briefly, BrdU was added to cells and incubated for another 12 hours. BrdU levels were then measured as absorbance at 450nm.

### **Western blotting**

Cultured HSASMCs were lysed and prepared for Western blot analysis using antibodies against Myocardin (R&D systems, MAB4028), STAT3 (Cell Signaling Technology, #4904), pSTAT3 (Cell Signaling Technology, #9145) and  $\beta$ -actin (Novus, #NB600-501). After incubation with appropriate secondary antibodies (ECL anti-rabbit and –mouse IgG, HRP-Linked Whole Ab for STAT3/pSTAT3 and myocardin, respectively, Thermo Fisher Scientific) coupled to horseradish peroxidase, blots were visualized using enhanced chemiluminescence (SuperSignal™ West Dura Extended Duration Substrate, Thermo Fischer Scientific). Protein expression was detected using Pierce ECL Western Blotting substrate reagent (Thermo Scientific) and ImageQuant LAS 4000 (GE Healthcare).

## Supplemental Results

### **Pemafibrate reduces SMC proliferation in artery culture ex vivo and promotes maturity of human coronary artery SMCs in vitro**

To evaluate and quantify the effects of pemafibrate on cell proliferation in arterial specimens, we performed organoid cultures of pig carotid arteries. Cell proliferation was assessed by immunostaining of Ki-67, a marker of cell proliferation. PDGF-BB increased the Ki-67-positive area (**Figure S4**). In PDGF-BB-treated arteries, pemafibrate reduced Ki-67 to levels similar to those present in the control arteries ( $p < 0.05$ ).

To probe further underlying mechanisms by which pemafibrate reduces stent neointima formation, we performed in vitro experiments with cultured human coronary artery SMCs. Consistent with the in vivo proteomics analysis, pemafibrate restored PDGF-BB-induced suppression of SMC differentiation markers including  $\alpha$ -SMA and calponin (**Figure S5**). STAT3 activation suppresses SMC differentiation induced by the transcriptional factor myocardin<sup>60</sup> and experiments demonstrated that pemafibrate suppressed PDGF-BB-induced phosphorylation of STAT3 and increased myocardin expression in human primary SMCs. Furthermore, pemafibrate suppressed SMC proliferation in culture at lower concentrations than that of fenofibric acid, the active metabolite of the conventional PPAR $\alpha$  agonist fenofibrate.

**Table S1.** IVUS and OCT measurements of coronary stents at day 7. Data shown as median (25<sup>th</sup>-75<sup>th</sup> percentile).

<b>Day 7: IVUS</b>			
	<b>Control (n=6)</b>	<b>Pemafibrate (n=6)</b>	<b>P-value</b>
<b>Stent expansion ratio (to distal reference diameter)</b>	1.3 (1.2-1.6)	1.3 (1.2-1.6)	0.94
<b>Mean stent diameter (mm)</b>	4.3 (3.9-4.7)	4.1 (3.9-4.5)	0.59
<b>Day 7: OCT</b>			
<b>Stent expansion ratio (to distal reference diameter)</b>	1.4 (1.2-1.5)	1.4 (1.2-1.5)	0.76
<b>Mean stent diameter (mm)</b>	4.3 (4.1-4.6)	4.1 (4.0-4.7)	0.92

**Table S2.** Body weight and laboratory measurements. Data shown as median (25<sup>th</sup>-75<sup>th</sup> percentile).

	<b>Control (n=7)</b>	<b>Pemafibrate (n=6)</b>	<b>P-value</b>
<b>Body weight Day 0, kg</b>	28.0 (22.0-32.0)	31.0 (23.0-34.8)	0.39
<b>Body weight, Day 28, kg</b>	42.0 (40.0-49.0)	43.0 (39.0-47.3)	0.44
<b>Difference (Day 28 – Day 0), kg</b>	17.0 (13.0-19.0)	14.5 (12.0-17.5)	0.40
<b>Triglycerides, mg/dL</b>	12.8 (7.7-21.7)	10.8 (6.0-20.0)	0.53
<b>AST, IU/L</b>	24.6 (24.3-31.3)	19.8 (17.0-29.2)	0.53
<b>ALT, IU/L</b>	38.5, (33.9-44.1)	44.2 (30.9-53.3)	0.49

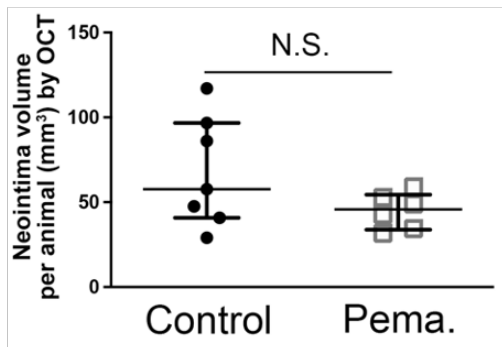
**Table S3.** Day 28 histology-based measures of neointima thickness, stent area, lumen area and neointima area between control and pemafibrate group. Data shown as median (25<sup>th</sup>-75<sup>th</sup> percentile). N=13 sections/animal analyzed.

	<b>Control (n=7)</b>	<b>Pemafibrate (n=6)</b>	<b>P-value</b>
<b>Neointima thickness (mm)</b>	0.53 (0.33-0.61)	0.33 (0.21-0.55)	0.26
<b>Stent area (mm<sup>2</sup>)</b>	10.1 (8.6-14.4)	10.7 (8.2-13.7)	0.9
<b>Lumen area (mm<sup>2</sup>)</b>	5.4 (4.1-6.7)	6.9 (4.5-10.4)	0.4

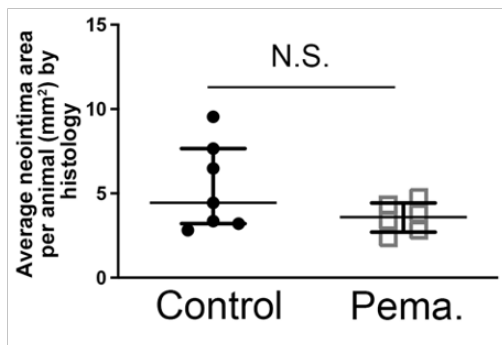
<b>Neointima area (mm<sup>2</sup>)</b>	4.4 (3.2-7.7)	3.6 (2.7-4.3)	0.4
--	---------------	---------------	-----

**Figure S1:**

**a**

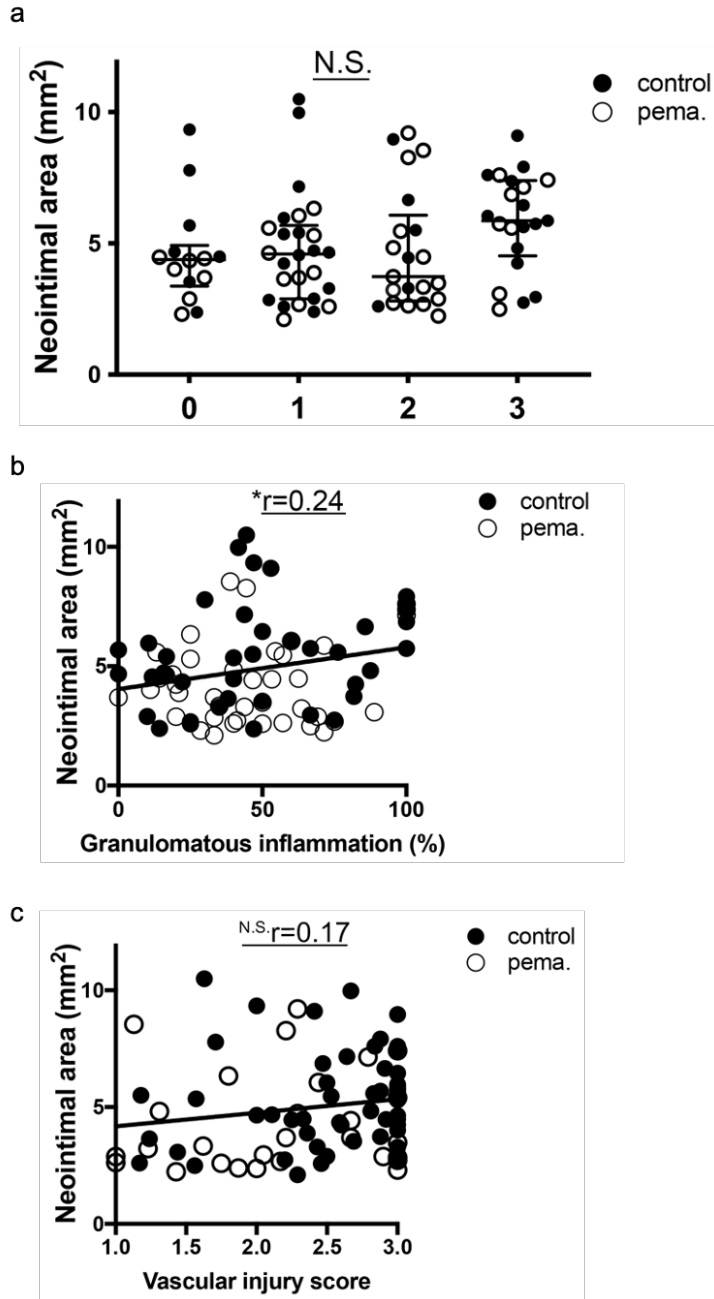


**b**



**a.** Day 28 in vivo OCT-measured average stent neointima volume per animal. In the pema fibrate group (n=6), the average neointimal volume tended lower than in control pigs (n=7) but did not reach statistical significance (p=0.366). Each dot represents one animal that was implanted with 2-3 stents; the neointimal volume from the average of these 2-3 stents is reported. **b.** Day 28 histology-measured average stent neointima area per animal (1 stent per animal, 12 sections per stent). Similar to the OCT results, in the pema fibrate group (n=6) the average neointimal volume also trended lower than the control group (n=7) but did not reach statistical significance (p=0.138). Each dot represents one animal; the average neointimal area per stent is reported. N.S., not significant. Horizontal lines and error bars indicate the median (25<sup>th</sup>-75<sup>th</sup> percentile).

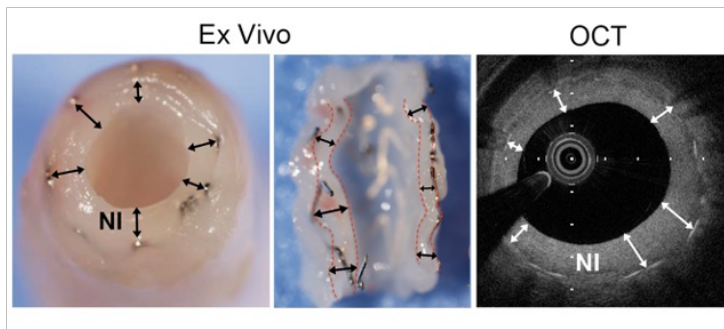
**Figure S2:**



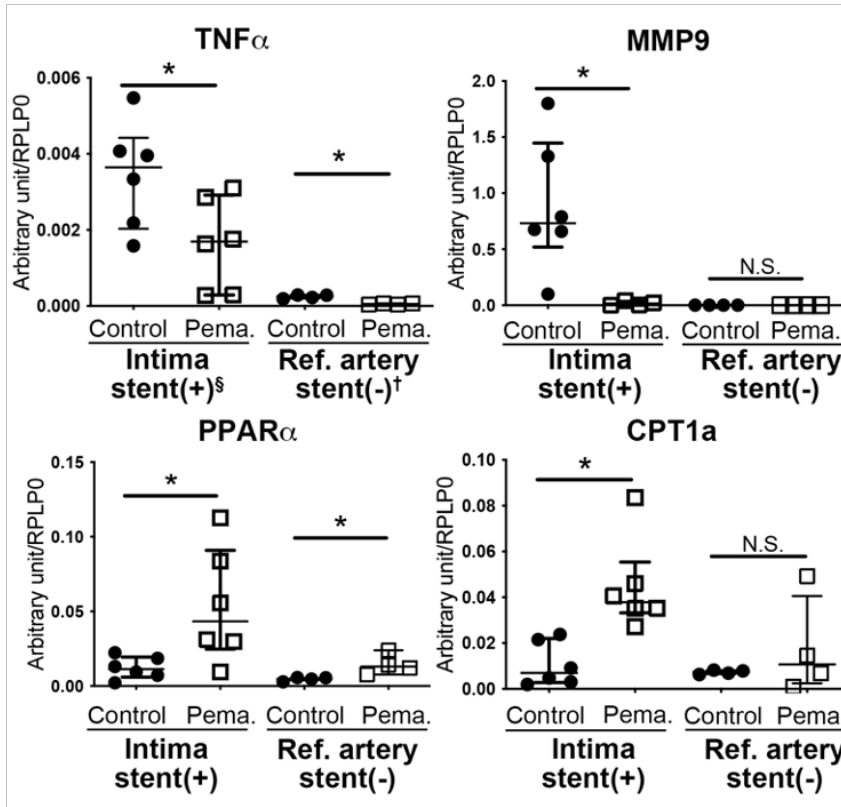
Day 28 histology analysis (82 sections analyzed). **a.** Relationship between the day 28 peri-strut inflammation score and stent neointima area (highest peri-strut inflammatory score per section was employed). Horizontal lines and error bars indicate the median (25<sup>th</sup>-75<sup>th</sup> percentile). **b.** Correlation between the day 28 granulomatous inflammation (%) and neointima area (mm<sup>2</sup>) per section ( $r=0.24$ ,  $p=0.03$ ). **c.** Relationship between the day 28 vascular injury score and stent neointima area ( $r=0.17$ ,  $p=0.13$ ).  $*p<0.05$ , N.S.: not significant, Pema.: Pema. fibrate.

**Figure S3: Molecular effects of pema. fibrate on inflammation and SMC differentiation in the arterial intima on day 28**

a

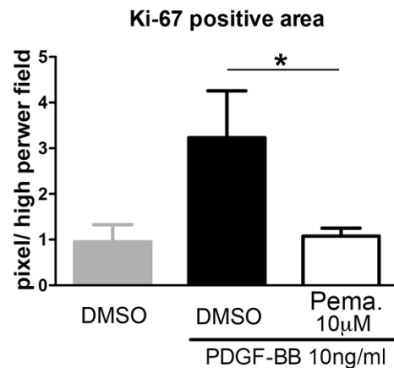
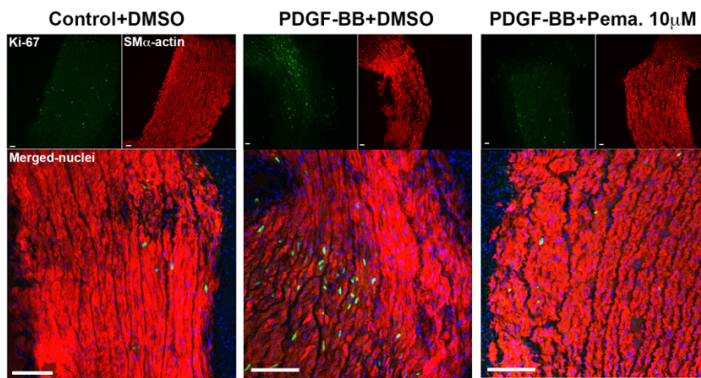


b



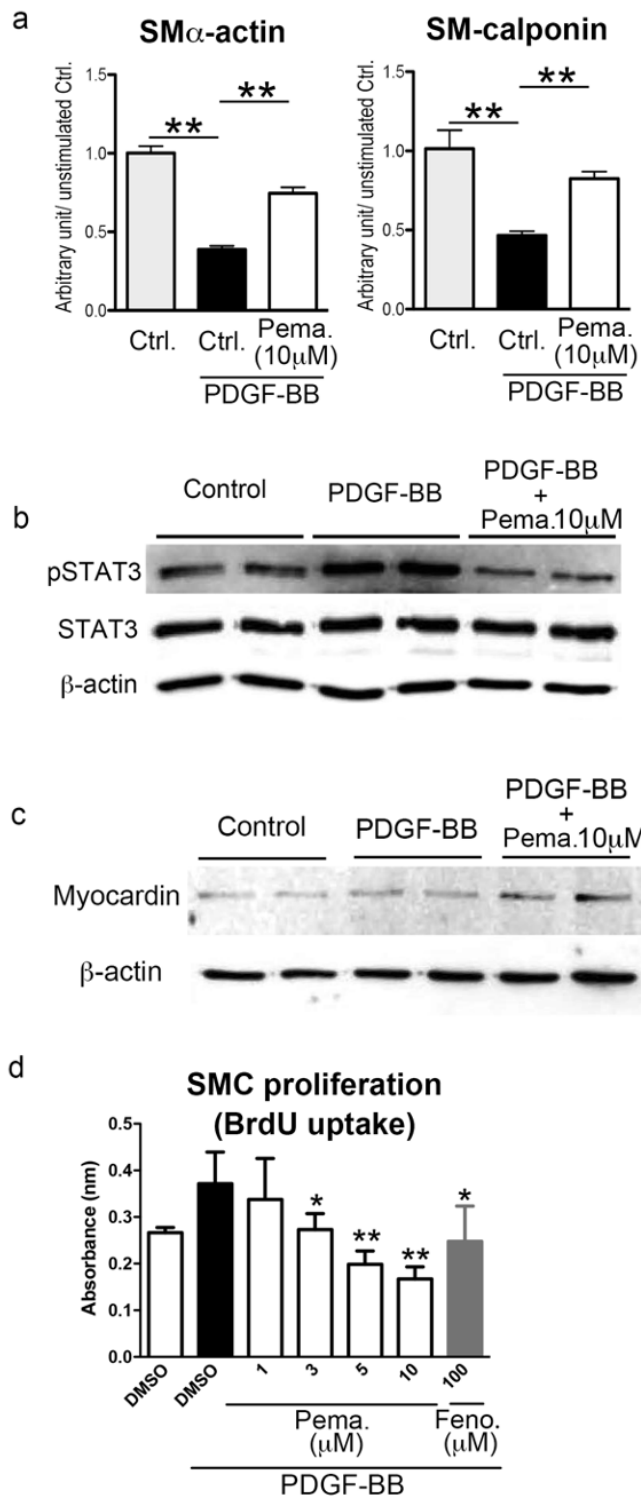
**a)** Neointima (NI) from day 28 resected stents (left and right panels, short axis ex vivo figure corresponding OCT image, respectively). Stented arteries were cut longitudinally and the intima was harvested (middle panel, longitudinal ex vivo figure). Black and white arrows indicate intima within the stent. **b)** Pemafibrate reduced mRNA expression of TNF and MMP-9 and enhanced PPAR- $\alpha$  gene and its downstream effector, CPT1a. \* $p < 0.05$ ; N.S., not significant,  $\S$ : intima in the stented lesion,  $\dagger$ : media in the non-stented lesion. Each dot depicts one stent. Horizontal lines and error bars indicate the median (25<sup>th</sup>-75<sup>th</sup> percentile).

**Figure S4: Pemafibrate suppresses PDGF-BB-induced cell proliferation in organoid cultures of carotid arteries**



Carotid arteries from control pigs underwent organoid culture experiments. Arterial Ki-67, a cellular marker of proliferation, was enhanced by PDGF-BB 10 ng/ml. Pema. (10  $\mu$ M) suppressed the induction of Ki-67 by PDGF-BB. \* $p < 0.05$ ; Pema.: Pema. Error bars indicate  $\pm$ SD; scale bar, 100 $\mu$ m.

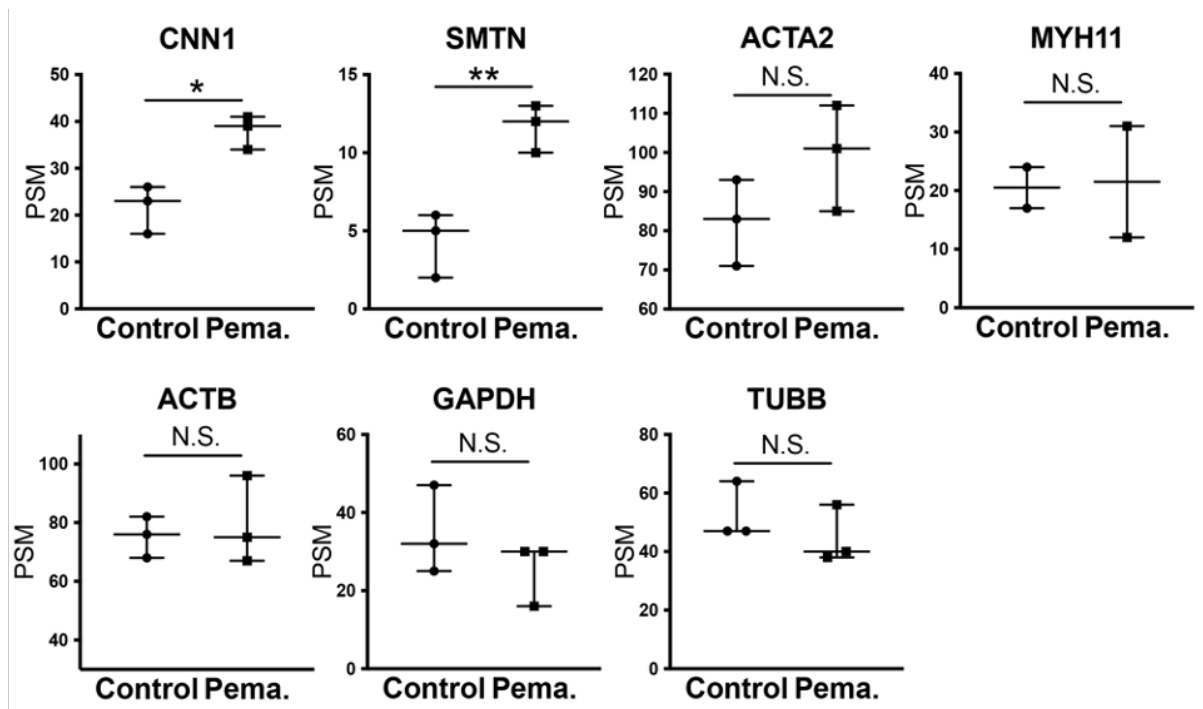
**Figure S5: Pema. maintains differentiation and suppresses proliferation in cultured human coronary artery SMCs**



**a)** Pemaifibrate rescued the expression of the more differentiated SMC markers SM  $\alpha$ -actin and SM calponin, which were suppressed by PDGF-BB (10ng/ml). **b)** Pemaifibrate suppressed PDGF-BB induced phosphorylation of STAT3. **c)** Pemaifibrate enhanced the expression of myocardin, the key transcriptional co-activator of SMC differentiation. **d)** Pemaifibrate suppressed SMC proliferation (BrdU uptake) in a dose-dependent manner. Its inhibitory effect was more potent in comparison to the conventional PPAR $\alpha$  agonist

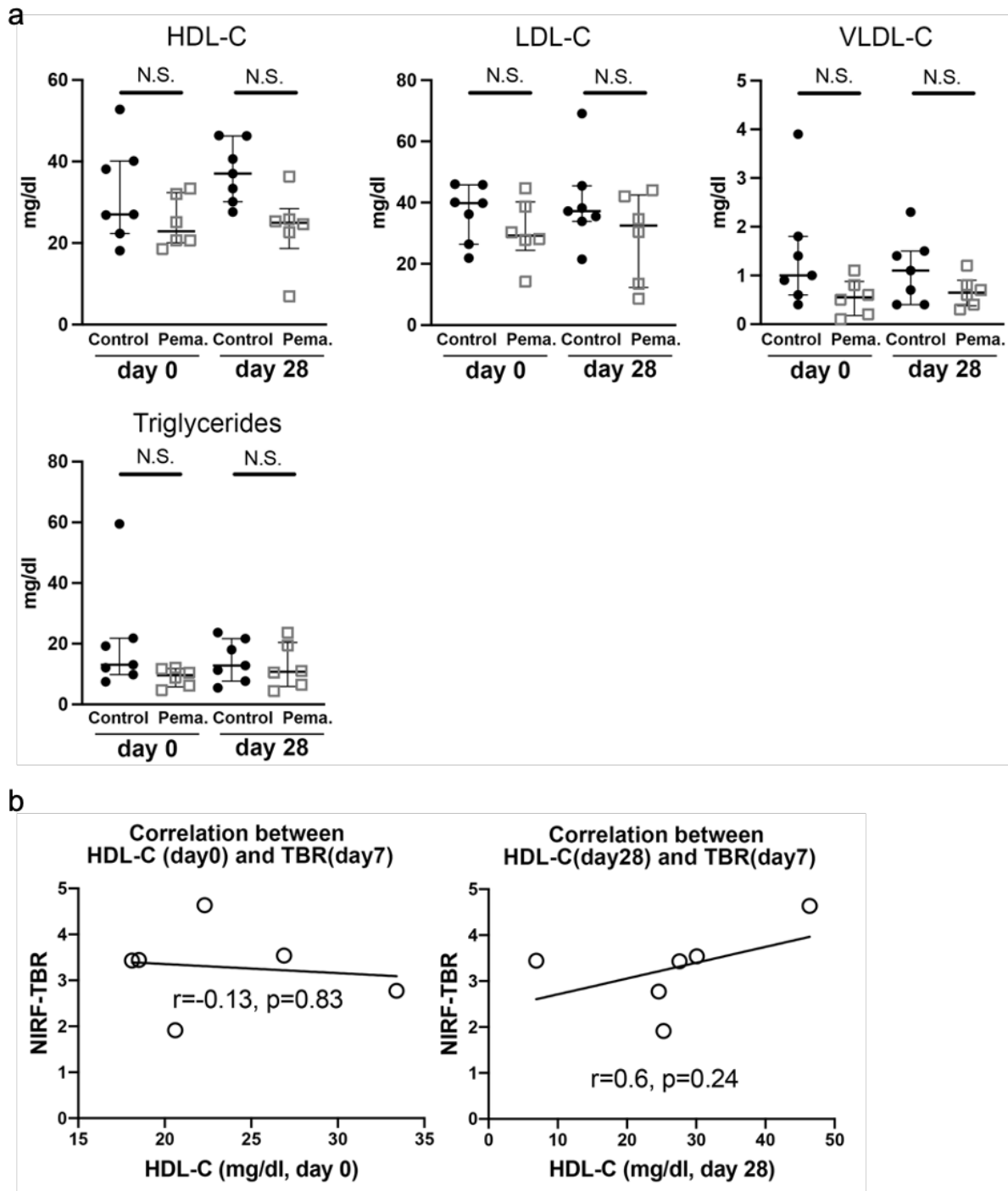
fenofibric acid. \* $p < 0.05$ , \*\* $p < 0.01$ , Pema.: Pemaifibrate; Feno.: fenofibric acid. Error bars indicate  $\pm$ SD.

**Figure S6: Proteomics analysis measured protein abundance of SMC differentiation markers of the intima in the stented lesion**



Relative protein abundance profiles (peptide spectrum matches, PSMs) of the harvested intimal tissues. SMC differentiation markers, including, calponin 1 (CNN1) and smoothelin (SMTN) were higher and SM alpha-actin (ACTA2) tended to be higher in the intima of stented lesions of pemaifibrate-treated animals than those of control animals, while the levels of housekeeping proteins, such as GAPDH,  $\beta$ -actin and  $\beta$ -tubulin, were similar. The levels of myosin heavy chain (MYH11) did not differ between groups. PSM: peptide spectrum matches, Pema.: pemaifibrate, \* $p < 0.05$ , \*\* $p < 0.01$ , N.S.: not significant. Each dot depicts one stent. Horizontal lines and error bars indicate the median (25<sup>th</sup>-75<sup>th</sup> percentile).

**Figure S7. Serum lipoprotein and triglyceride levels on day 0 and day 28, and relationship of HDL levels to NIRF inflammation.**



Pemafibrate animals began treatment on day -7. (a) HDL-C, LDL-C, VLDL-C, and triglyceride levels at day 0 and day 28, for both control and pemafibrate animals. Horizontal lines and error bars indicate the median (25<sup>th</sup>-75<sup>th</sup> percentile). (b) No significant correlation was observed between the day 7 TBR NIRF inflammation signal and (left) the day 0 HDL-C level or the (right) day 28 HDL-C level. HDL=High-Density Lipoprotein, LDL=Low-Density Lipoprotein, VLDL=Very-Low-Density Lipoprotein, TBR=Target-to-Background Ratio, NIRF=Near-infrared fluorescence.